Brainwide blood volume reflects opposing neural populations

Agnès Landemard[1], Michael Krumin[1], Kenneth D Harris[2], and Matteo Carandini[1]

Abstract

The supply of blood to brain tissue is thought to depend on the overall neural activity in that tissue, and this dependence is thought to differ across brain regions and across levels of arousal. Studies supporting these views, however, measured neural activity as a bulk quantity, and related it to blood supply following disparate events in different regions. Here we measure fluctuations in neuronal activity and blood volume associated with the same events across the mouse brain, and find that their relationship is consistent across brain regions but differs in two opposing brainwide neural populations. Functional Ultrasound Imaging (fUSI) revealed that whisking, a marker of arousal, is associated with brainwide fluctuations in blood volume. Simultaneous fUSI and Neuropixels recordings in cortex and hippocampus showed that neurons that increase vs. decrease activity with whisking have distinct hemodynamic response functions. Brainwide Neuropixels recordings revealed that these two opposing populations are present in the entire brain. When summed, their contributions predicted blood volume across brain regions better than predictions from bulk neural activity. The mouse brain thus contains two neural populations with opposite relation to brain state and distinct relationships to blood supply, which together account for brainwide fluctuations in blood volume.

Introduction

The blood supply to the brain is tightly correlated with neuronal activity[1-5]. This neurovascular coupling is usually described by a positive hemodynamic response function (HRF) that acts as a filter on the neural activity. Filtering the neural activity measured in a local region with the HRF provides a reasonable prediction of the blood supply in that local region[6-12].

There is debate, however, about whether neurovascular coupling is consistent across brain regions[5,13]. Weaker HRFs have been reported in olfactory bulb[14], somatosensory thalamus[15], and frontal cortex[16]. Some studies even reported negative HRFs, such as in somatosensory cortex (ipsilateral to a sensory stimulus[17]) or in striatum[18]. Others argued that the HRFs are always positive (with decreases in blood supply stemming from decreases in firing rate[19]), and are consistent across brain regions[10,20].

Moreover, neurovascular coupling might differ across brain states[5]. For instance, in mouse somatosensory cortex the correlation between blood supply and neural activity was reported to be stronger during sensory stimulation than at rest[21], and stronger in NREM sleep than during wakefulness or REM sleep[22]. In macaques, moreover, neurovascular coupling was reported to be stronger when the animal rests[20]. Furthermore, changes in attention[23] or anticipation[11,24] seem to affect blood supply more than local neural activity. Perhaps these factors engage vascular mechanisms that do not depend only on neuronal firing[2].

[1]UCL Institute of Ophthalmology, University College London; [2]UCL Queen Square Institute of Neurology, University College London

However, previous studies of neurovascular coupling summarized neural activity with bulk measures, which cannot distinguish the potentially different correlates of different neurons. Bulk measures of neural activity provide better predictions of blood supply than individual neurons[25]. However, the pathways that relate neural activity to blood supply are complex and may well differ across cell types[5,26]. For example, the coupling between blood supply and activity might differ in neurons vs. glia[27] or in inhibitory vs. excitatory neurons[28,29]. Across the brain, there may be populations of neurons that have different patterns of activity and different coupling to blood supply, which would not be distinguishable in bulk measurements of neural activity.

Moreover, studies of neurovascular coupling measured neural activity in different regions in relation to different events. Studies focused on different regions, such as olfactory bulb[14], somatosensory cortex[15], or frontal cortex[16], measured neural activity with respect to different events, such as the delivery of an olfactory or somatosensory stimulus, or the onset of spontaneous running. Their results, therefore, are hard to compare and to assemble into a unified view of neurovascular coupling across the brain.

To overcome these limitations, we measured brainwide blood volume and brainwide neural activity in relation to brainwide neural events. We focused on the neural events related to spontaneous behavior, because they span multiple brain regions[30-32], and particularly on whisking, a reliable marker of arousal in rodents[12]. Functional Ultrasound Imaging[33] (fUSI) revealed that whisking is associated with stereotyped, brainwide changes in blood volume, which predict blood volume changes associated with arousal events. Simultaneous fUSI and Neuropixels recordings[10] revealed that neurons that increase vs. decrease activity with whisking[30,34,35] have distinct hemodynamic response functions (HRFs). Brainwide recordings of 18,791 neurons[36] with Neuropixels probes[37] revealed that these opposing populations coexist in every brain region. When the different HRFs are applied to the activity of the two populations, and the results are summed, the resulting prediction captures the brainwide fluctuations in blood volume better than the bulk local activity. These results indicate that neurovascular coupling is consistent across brain regions and levels of arousal, but is different in two brainwide neural populations with opposite relation to brain state.

Results

To measure the changes in blood volume associated with spontaneous behaviors, we used functional Ultrasound Imaging[33] (fUSI). In each session, we measured cerebral blood volume in a coronal imaging plane, simultaneously capturing its dynamics in many brain regions (Figure 1a). We varied the imaging plane across sessions, so that all planes together covered the posterior half of the cerebrum (cortex, hippocampal formation, striatum, and pallidum), all of the interbrain (thalamus, hypothalamus, and zona incerta), most of the midbrain (including the substantia nigra and the superior colliculus), and part of the pons (Table S1). We aligned the imaging planes to the Allen Common Coordinate Framework Atlas[38], assigned each voxel to a brain region, and computed the median activity across voxels within each region. Mice were head-fixed but free to run on a wheel. We monitored their behavior with infrared cameras as they spontaneously went through varying states of arousal. These fluctuations in arousal were marked by bouts of whisking[30,32,39] that were often accompanied by locomotion[40] (Figure 1b) and that correlated with fluctuations in blood volume in multiple brain regions (Figure 1c).

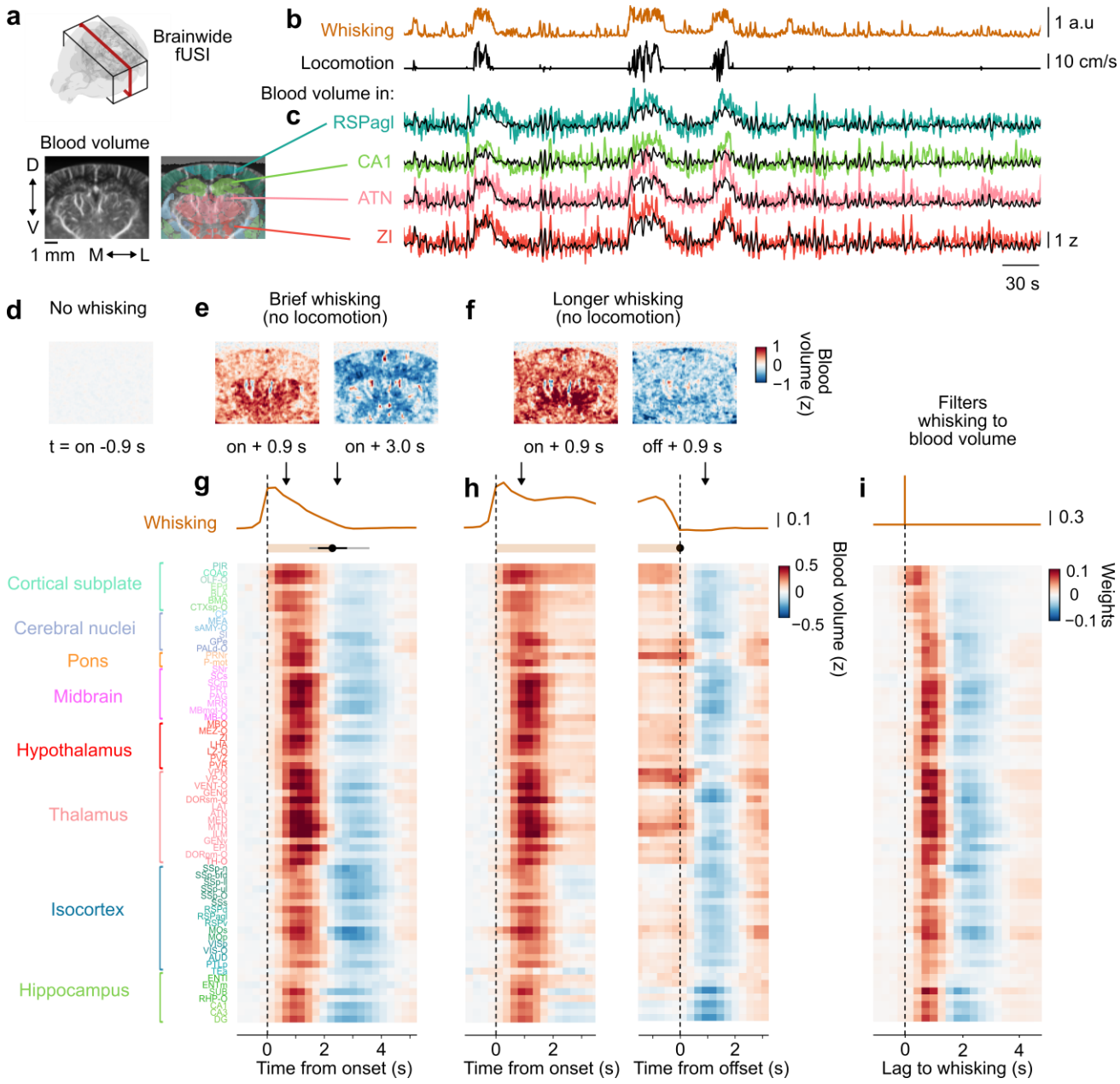

Figure 1. **Brainwide blood volume is strongly modulated by arousal events. a.** We measured blood volume in coronal planes using functional ultrasound imaging (fUSI), varying the imaging planes (*red outline*) across sessions to image a larger portion of the brain (*black outline*). Imaged volumes were aligned to the Allen Brain Atlas and voxels were averaged within brain regions (*colors*). **b.** Behavioral measurements in a snippet from a typical session, showing prolonged whisking bouts accompanied by locomotion, and briefer whisking bouts without locomotion. **c.** Fluctuations in blood volume for the same example session in four example regions in isocortex (RSPagl), hippocampus (CA1), thalamus (ATN) and zona incerta (ZI). See Table S1 for abbreviations. Black traces show predictions of blood volume from whisking (see **i**, Figure S3). **d.** Average blood volume 0.9 s before the onset of whisking bouts in the example session. Each voxel is baseline-subtracted using a window of 0.5-2 s before whisking onset. **e.** Average blood volume for brief whisking bouts (1.3-3.5 s) not accompanied by locomotion, 0.9, and 3.0 s after whisking onset. **f.** Average blood volume for longer whisking bouts (>3.5 s) not accompanied by locomotion, 0.9 s after whisking onset (*left*), or offset (*right*). **g.** Average changes in blood volume throughout all imaged regions during brief whisking bouts (1.3-3.5 s, average = 2.2 s) without locomotion. Arrows indicate the times of the images in **e.** The shaded area below whisking indicates average bout duration, with time of offset indicated in black (average +/- one standard deviation), and the range of possible offset times in grey. Colors indicate z-scored blood volume. **h.** Same, for longer whisking bouts without locomotion (> 3.5 s, average = 12.1 s), aligned to bout onset (*left*) and offset (*right*). See Figure S1 for whisking bouts associated with locomotion. **i.** Best-fitting filters obtained to fit blood volume from whisking, for all brain regions (see Figure S2 and Figure S3 for prediction details). These filters model changes in blood volume for a Dirac delta function of whisking. Example predictions are shown in **a** (*black traces*).

Arousal events were associated with widespread and dynamic changes in blood volume. These events were characterized by whisking and locomotion. Locomotion was always associated with whisking and was accompanied by strong, sustained increases in blood volume (Figure 1b, c, Figure S1). Whisking also occurred in the absence of locomotion, so we adopted it as a more sensitive assay of arousal. In a typical session, brief bouts of whisking led to a widespread increase in blood volume followed by a decrease (Figure 1d, e). Longer bouts led to a similar pattern, with decreases in blood volume occurring at whisking offset (Figure 1f).

Brainwide measurements of blood volume established that correlates of whisking were present in the whole brain. We repeated our fUSI measurements in 5 mice and 138 sessions (101 hours of imaging) across multiple coronal planes, and we combined the results for each brain region. Brief whisking bouts (1.3-3.5 s, without locomotion), led to an almost simultaneous increase in blood volume in the entire brain, followed by an almost simultaneous decrease around 2 s after the bout began (Figure 1g). Longer whisking bouts led to a longer brainwide increase in blood volume, followed by a similar simultaneous decrease when the bout stopped (Figure 1h). These effects were similar across brain regions, with occasional differences in amplitude and dynamics. For example, hippocampus and some regions of isocortex only showed a transient increase lasting ~2 s, followed by a decrease even while whisking continued; ventral regions such as amygdala and olfactory areas tended to activate earlier than the others at the onset of whisking bouts (Figure 1g, h).

These brainwide fluctuations in blood volume could be reproduced by applying a biphasic filter to the whisking timecourse. We sought to capture the effect of whisking on each region's blood volume throughout time regardless of specific whisking events. To this end, we used linear regression to obtain filters that predict that region's blood volume from whisking (Figure 1i, Figure S2). The resulting predictions accounted for a large fraction of the variance in blood volume across states of arousal, from stillness to locomotion, and across multiple regions (Figure 1c, Figure S3). Thus, brainwide fluctuations in blood volume can be predicted by applying a biphasic filter to an arousal factor indexed by whisking.

We next investigated the neural basis of the whisking-related changes blood volume. We used simultaneous recordings of hundreds of neurons in visual cortex and hippocampus with Neuropixels and blood volume with fUSI[10] (Figure 2a). We binned spikes to the same temporal resolution as the fUSI data (300 ms time bins) and computed the overall firing rate of the neurons, along with whisking and blood volume in visual cortex (Figure 2b).

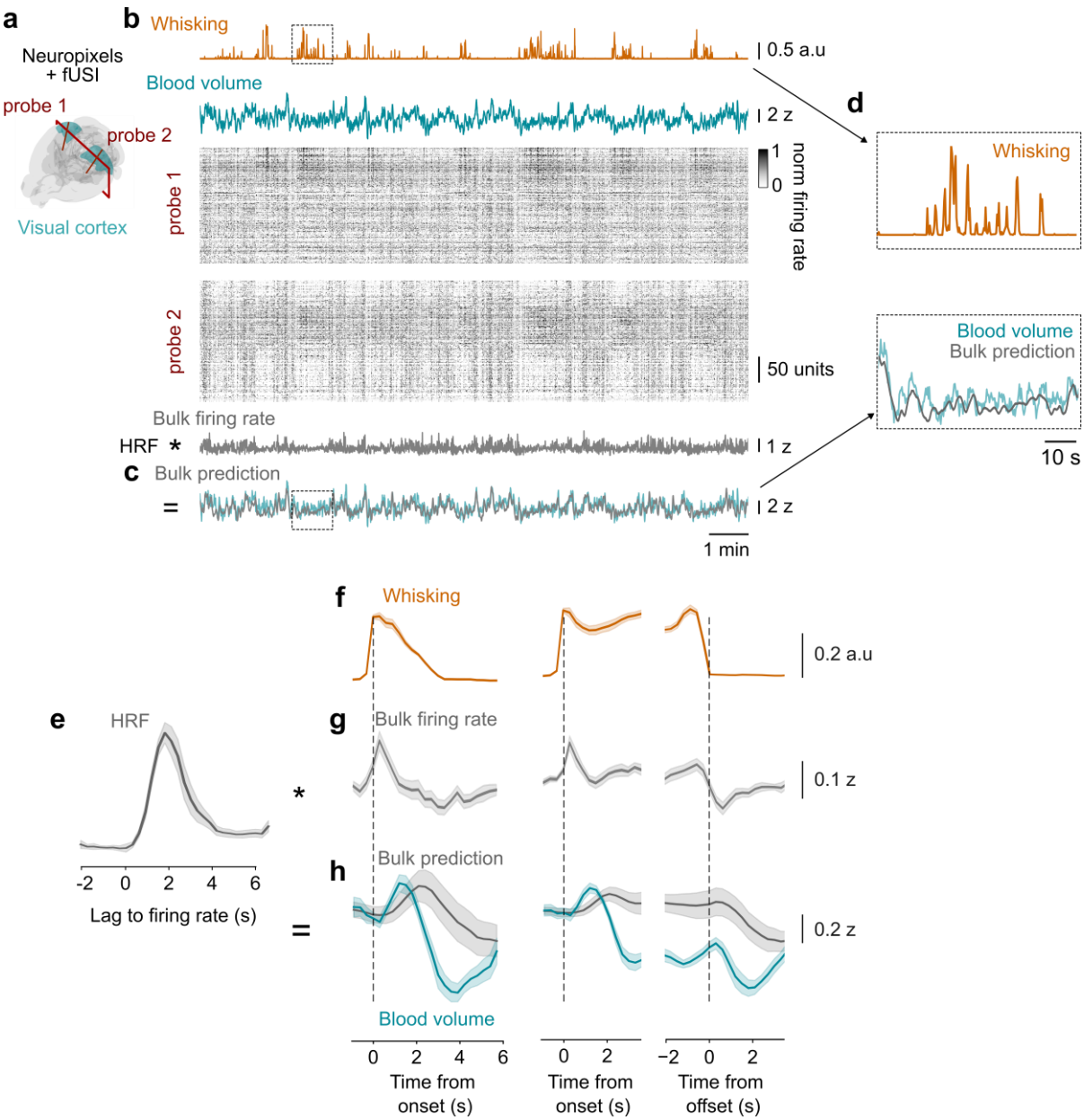

Figure 2. **Bulk firing rate poorly predicts changes in blood volume with whisking events**. **a.** While imaging blood volume with fUSI, we used Neuropixels probes to record from hundreds of neurons in visual cortex and hippocampus[10]. **b.** Snippet from a typical recording session in visual cortex, with whisking (*gold*), blood volume (*cyan*) along with the normalized firing rate of all neurons recorded bilaterally across two probes in visual cortex. The firing rate for each neuron is divided by the 95th percentile of firing rate across time. Neurons are sorted by depth on each probe. Bulk firing rate (*grey*) is obtained by taking the average over all neurons. **c.** The filtered bulk firing rate (*grey*) to predict blood volume (*cyan*) throughout the session. **d.** Zoomed-in snippet of the session in **b-c**, showing small whisking bouts (*gold*) along with blood volume (*cyan*) and predictions from bulk firing rate (*grey*). **e.** The best-fitting filter to predict blood volume from bulk firing rate. **f.** We identified whisking bouts and looked at brief (*left*) and longer whisking bouts, aligned to onset (*middle*) or offset (*right*). **g.** Average changes in bulk firing rate during whisking events. **h.** Average changes in blood volume during whisking events (*cyan*), and prediction from bulk firing rate in visual cortex (*grey*). **e-h** show results averaged across all recording sessions in visual cortex (see Figure S4 for similar results in hippocampus).

We first attempted to predict the changes in blood volume from the local bulk firing rate, and failed to capture the correlates of whisking. Following established precedent[6-12], for each recording session, we fit a linear filter to predict blood volume from the average firing rate. As expected[10], the best-fitting filter provided good overall predictions of blood volume (Figure 2c). Across sessions the best-fitting filter was monophasic and peaked 1.8 s after neural activity (Figure 2e), consistent with the standard HRFs that have been previously obtained from bulk

neural activity in mice[10,41,42]. However, closer inspection revealed that the prediction tended to be sluggish, failing to capture the fastest dynamics of spontaneous blood volume (Figure 2d). This limitation was particularly clear during whisking events. The bulk firing rate measured during whisking events showed an increase followed by a smaller decrease (Figure 2f, g). This slightly biphasic response is in principle consistent with the biphasic response we observed in simultaneously recorded blood volume. However, convolution with the HRF (Figure 2e) smoothed this feature out, failing to reproduce the biphasic changes in blood volume seen during whisking events (Figure 2h). Thus, a linear filter on average neural activity could not properly account for changes in blood volume during whisking events. To account for brainwide blood volume, it might be necessary to consider more than one dimension of neural activity.

Closer inspection of the neural data revealed two populations of neurons with opposite modulation by arousal. Consistent with previous measurements[30], we found that neurons differed substantially in their relation to whisking: some neurons correlated positively with whisking and some neurons correlated negatively (Figure 3a, b). We refer to these two opposing populations as arousal+ and arousal– neurons. We hypothesized that considering this heterogeneity could provide a better prediction of blood volume.

The firing rates of the two opposing populations provided good estimates of the local blood volume. We designed a model where the blood volume in a region reflects not just the bulk neural activity but rather the activity of the two opponent populations of arousal+ and arousal– neurons, each acting with its own HRF. For each session, we filtered the activity of arousal+ neurons and of arousal– neurons with the best-fitting filters to obtain a prediction of blood volume (Figure 3c). The resulting filters were positive and monophasic, but with different peak times and widths (Figure 3e): the filter for arousal+ neurons peaked earlier (1.2 s after neural activity) and was narrower (1.2 s full width at half height), whereas the filter for arousal– neurons peaked later (2.1 s after neural activity) and was wider (1.8 s). Compared to the bulk prediction, this combined prediction was better able to track the observed fluctuations in blood volume, even in the absence of whisking (Figure 3d). The prediction from arousal+ and arousal– neurons provided a good account of the blood volume fluctuations associated with whisking events (Figure 3f). At whisking onset, the activity of arousal+ neurons increased (Figure 3g), while the activity of arousal– neurons decreased (Figure 3h). The combined prediction from these two populations captured the characteristic biphasic changes in blood volume seen during whisking events (Figure 3i). Indeed, after the onset of whisking the blood volume first increased due to the increase in activity of arousal+ neurons and later decreased due to the delayed decrease in activity of arousal– neurons. More generally, regardless of whisking events, the firing rates of the two opposing populations provided better estimates of blood volume than the bulk firing rate: their predictions had higher coherence with the measured blood volume at all frequencies, both in visual cortex ($p = 0.015$ across frequencies, Figure 3j) and in hippocampus ($p = 0.002$, Figure 3k, Figure S4). This improvement was not restricted to periods of strong whisking: it was present even during periods of relative quiet (Figure S5).

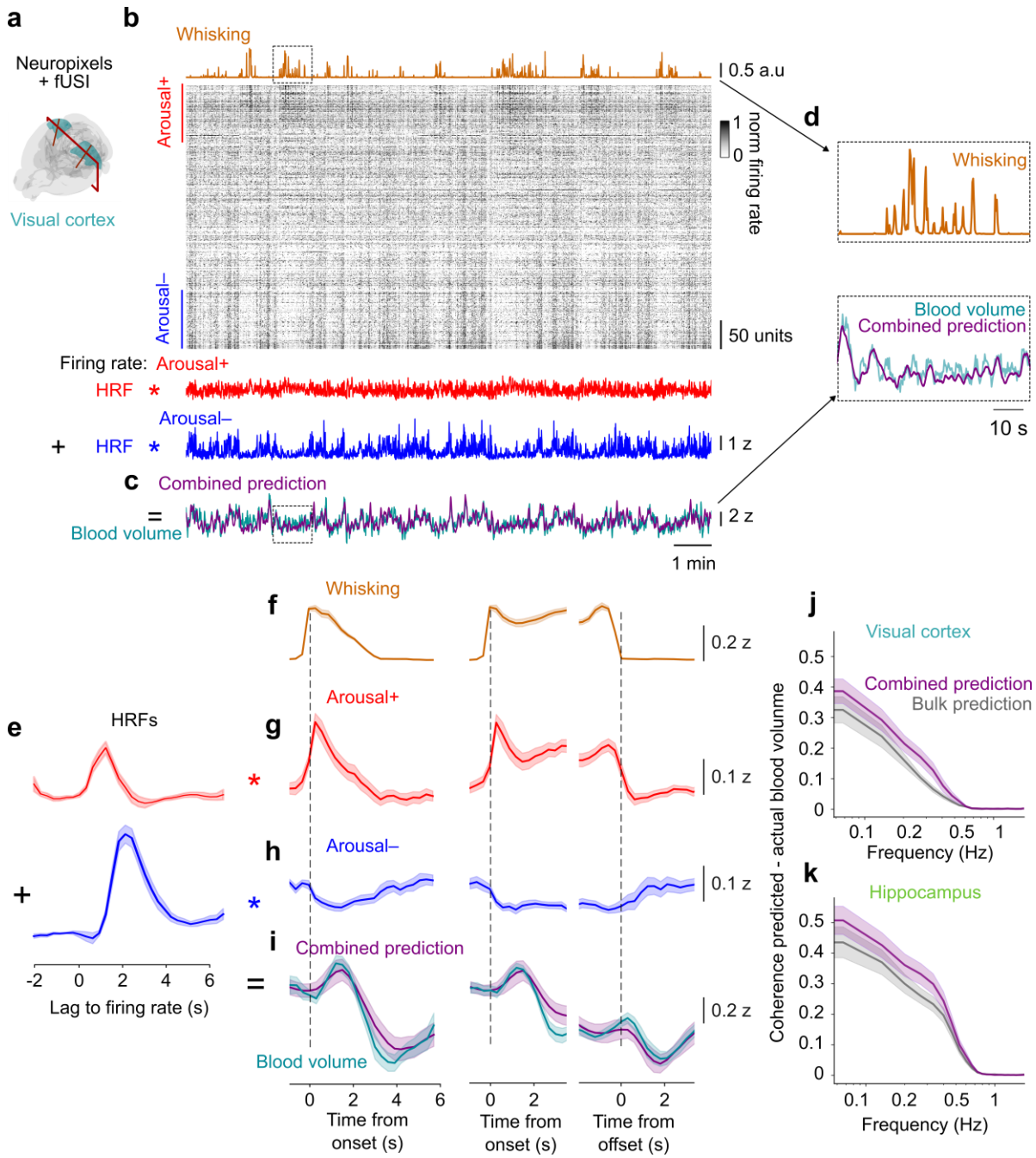

Figure 3. **The firing rate of two arousal–defined neural populations best predicts blood volume**. **a.** We used the same simultaneous Neuropixels-fUSI recordings (Figure 2, Ref[10]) in visual cortex and hippocampus. **b.** *Top:* Snippet from a typical recording session in visual cortex (same as in Figure 2), with whisking (*gold*) along with the normalized firing rate of all neurons recorded in visual cortex sorted by correlation with whisking. The correlation is computed on half of the recording session, and the example snippet is taken from the other half. The firing rate for each neuron is divided by the 95th percentile of firing rate across time. Bars indicate arousal+ neurons (*red*, correlation with whisking > 0.05), and arousal– neurons (*blue*, correlation with whisking < -0.05). *Bottom:* Average firing rate for arousal+ neurons (*red*), and arousal– neurons (*blue*). The firing rate of each neuron is z-scored before averaging. **c.** Simultaneously measured blood volume (*cyan*), along with the combined prediction obtained from the firing rate of arousal+ and arousal– neurons. **d**. Zoomed-in snippet of the session in **b-c**, showing small whisking bouts (*gold*) along with blood volume (*cyan*) and the combined prediction (*purple*). **e**. The best-fitting filters to predict blood volume from arousal+ (*red*)and arousal– (*blue*) neurons. **f**. Traces of whisking for brief (*left*) and longer whisking events, aligned to onset (*middle*) or offset (*right*). **g**. Average changes in firing rate for arousal+ neurons during whisking events. **h**. Same, for arousal– neurons. **i.** Average change in blood volume during whisking events (*cyan*), and prediction from arousal+ and arousal– neurons in visual cortex (*purple*). Data presented in **e-i** is averaged across all recording sessions in visual cortex (see Figure S4 for results in hippocampus). **j.** Coherence between predicted and actual blood volume for the predictions from bulk firing rate (*grey*, presented in Figure 2) or from arousal+ and arousal– neurons (*purple*), in visual cortex. Shaded area shows the s.e. across sessions. **k**. Same, for recordings in hippocampus.

The changes in blood volume seen in visual cortex and hippocampus during whisking events, therefore, are best explained by the activity of two opposing populations of neurons, each with its own hemodynamic response function. The improved performance of the predictions from the two opposing populations cannot be explained by having more free parameters because the fits were performed with cross-validation (see Methods). Moreover, the improvement was specific to those two populations of neurons: it was not present when using two random populations of neurons (Figure S6). Finally, we tested whether a biphasic HRF would provide a good account of blood volume based on average firing rate only. To do so, we computed a biphasic HRF from the difference between the HRF for arousal+ neurons (Figure 3e, top), and the HRF for arousal– neurons (Figure 3e, bottom), with different weights. Applying these filters to the average firing rate was not sufficient to recapitulate the changes in blood volume during whisking events nor to reach similar levels of accuracy as the model from the two populations (Figure S7). Thus, the two populations of arousal+ and arousal– neurons provide a superior account of blood volume, that cannot be achieved from bulk firing rate alone.

To test whether a similar model applied in other brain regions, we turned to recordings with Neuropixels probes[37] across the entire mouse brain[36]. In these recordings, each brain region is covered by multiple probe insertions. We focused on the periods after the end of decision-making task sessions, when the mice rested passively (n = 324 recordings from 108 mice), and exhibited fluctuations in arousal marked by whisking. Again, we binned spikes to the same temporal resolution as the fUSI data (300 ms time bins), and we assigned neurons to brain regions using the same mapping (e.g., Figure 4a).

Arousal+ and arousal– neurons were present throughout all brain regions. As in the simultaneous fUSI-Neuropixels measurements (Figure 3), in the visual cortex, fluctuations in arousal drove two opposing populations of neurons[30], increasing activity in arousal+ neurons and decreasing it in arousal– neurons (Figure 4a). Similar results were seen in the whole brain (Figure 4b, c): averaged across regions, about half of the neurons (47±12%, s.d. across 55 regions) correlated positively with whisking, and a smaller but substantial fraction (16±7%) correlated negatively with whisking. The relative abundance of arousal+ and arousal– neurons varied between regions (Figure 4c). For instance, arousal+ neurons were more abundant in thalamus (61±10%, s.d. across 12 thalamic regions, e.g. Figure 4a) and arousal– neurons were more abundant in auditory cortex (Au, 27% of neurons) and secondary somatosensory cortex (SSs, 35% of neurons).

These opponent neural populations both showed monophasic responses to arousal events. In each brain region, the firing of arousal+ and arousal– neurons followed a roughly similar timecourse, with opposite signs (Figure 4d, e). Their contributions thus tended to cancel out in the average firing rate (Figure S8), particularly in regions where arousal– neurons were more frequent, such as hippocampus. The two populations, however, showed subtly distinct dynamics: the activity of arousal+ neurons peaked 0.11±0.02 s (s.e. across 55 regions) after whisking onset (Figure 4d). The activity of arousal– neurons peaked 0.78±0.26 s after whisking onset (Figure 4e), significantly later than arousal+ neurons ($p = 8e\text{-}6$, Wilcoxon signed-rank test across regions).

The two opposing neural populations provided a better account of blood volume across the brain than the bulk neural activity. The bulk firing rate measured after whisking onset correlated significantly with the blood volume measured across regions ($r = 0.44$, $p = 0.0008$, Figure 5a), but underestimated the blood volume changes seen in certain midbrain regions and overestimated those seen in certain cortical regions. Blood volume across regions showed a stronger correlation with the relative proportion of arousal+ vs. arousal– neurons ($r = 0.63$, $p = 3.3e\text{-}7$, Figure 5b), with more accurate estimates of blood volume changes for many brain regions, especially in the midbrain and cortex.

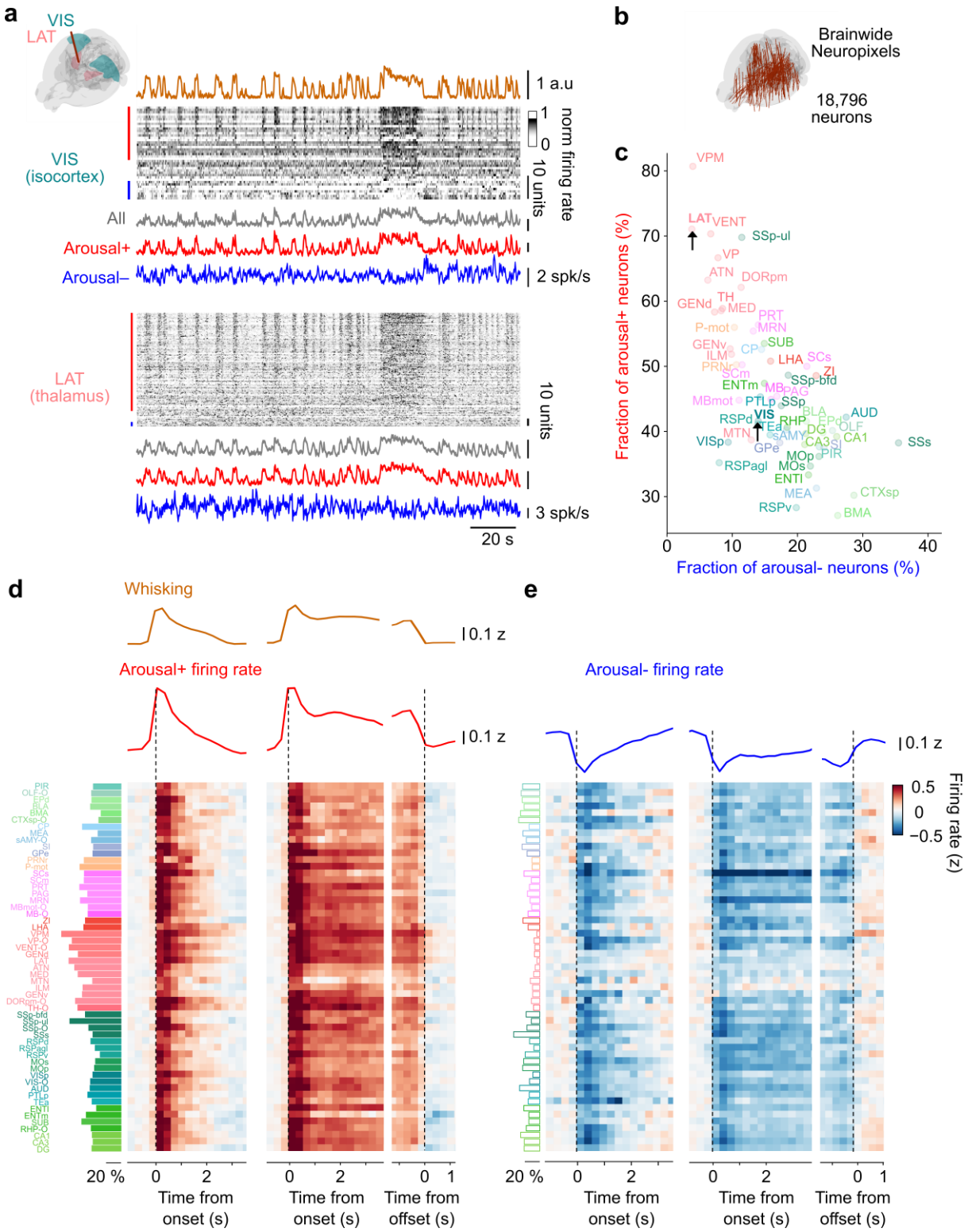

Figure 4. **The two arousal–defined neural populations are present throughout the brain. a.** Example Neuropixels recording with neurons in visual cortex (VIS, *top*) and lateral group of the dorsal thalamus (LAT, *bottom*) [36], showing the firing rate of all recorded neurons for each region, ordered based on their correlation with whisking (*gold*). The firing rate for each neuron is divided by the 95th percentile of firing rate across time. Bars indicate arousal+ neurons (*red*, correlation with whisking > 0.05), and arousal– neurons (*blue*, correlation with whisking < -0.05). *Bottom*: Average firing rate for all (*grey*), arousal+ (*red*) and arousal– neurons (*blue*). The firing rate of each neuron is z-scored before averaging. Arousal+ and arousal– neurons are identified on half of the data, and activity is shown for a snippet of the other half. **b.** A map with all the Neuropixels probe insertions that we included for analysis (18,791 neurons across the brain[36]). **c.** Comparison of the fraction of arousal+ and arousal– neurons across regions. Arrows indicate the example regions shown in **a**. **d.** *Left*: Proportion of arousal+ neurons across regions. *Right*: Average firing rate during whisking events for arousal+ neurons within each region. Activity is aligned to the onset of brief bouts (*left*), the

onset (*middle*) or the offset (*right*) of long bouts. The average activity of arousal+ neurons across regions peaked at the time of whisking onset (0 s offset, *dashed line*). **e**. Same, for arousal– neurons. The average activity of arousal– neurons across regions hit its lowest mark after whisking onset (*dashed line*).

Indeed, using the firing rate of arousal+ and arousal– neurons improved the ability to predict brainwide blood volume during whisking events. To test this, we used the bulk model (Figure 3) and the combined model (Figure 4) to predict whisking-related blood volume throughout the brain. For the bulk prediction, we convolved the bulk firing rate obtained with the brainwide Neuropixels recordings (Figure S8) with the HRF obtained for bulk firing rate in the simultaneous Neuropixels and fUSI recordings (Figure 2e, Figure S4, averaged across all measurements in visual cortex and hippocampus). We followed the same procedure to obtain combined predictions of blood volume from of arousal+ and arousal– populations for each brain region, this time applying the filters found for arousal+ and arousal– neurons (Figure 3e) to the firing rate of these populations in each region (Figure 4d, e). We scaled the contributions of arousal+ and arousal– populations based on the relative sizes of these populations in each region, and we summed them to obtain a combined prediction of whisking-related changes in brainwide blood volume. The bulk prediction completely missed the biphasic dynamics and the delays of blood volume following whisking events(Figure 5c) while the combined prediction well recapitulated these characteristics (Figure 5d). The combined prediction thus largely outperformed the bulk prediction, leading to a smaller error in most brain regions (Figure 5e).

Discussion

By combining three datasets acquired in different mice with different techniques, we obtained high-quality predictions of fluctuations in blood volume across the mouse brain. Large-scale fUSI measurements revealed brainwide fluctuations in blood volume that could be predicted from whisking. Simultaneous fUSI and Neuropixels recordings revealed that neurons that increase vs. decrease activity with whisking have distinct, positive hemodynamic response functions (HRFs). Brainwide Neuropixels recordings revealed that these two populations are present in the whole brain. Filtering their firing rates with their HRFs and combining the results provided good accounts of brainwide changes in blood volume with arousal, outperforming the predictions from bulk firing rate. Thus, neurovascular coupling appears to reflect not the bulk firing rate, but rather the firing rates of two brainwide neural populations with opposite relation to arousal state.

This finding extends previous studies of neurovascular coupling, without contradicting them. Indeed, these studies could not have observed the two opposing populations, because they obtained a single measure of bulk neuronal activity, such as the local field potential or the overall firing of a local population.

Our results indicate that whisking is a good predictor of brainwide fluctuations in blood volume. In addition to whisking, arousal is indexed by multiple behavioral correlates such as pupil dilations and locomotion[12,43-46]. Here we considered whisking and locomotion, and we found that whisking could explain a substantial part of fluctuations in blood volume throughout the brain, including during times of locomotion. Since locomotion is always preceded and accompanied by strong whisking, whereas whisking can occur without locomotion, whisking is a more interesting predictor for arousal-related fluctuations than locomotion. Pupil dilations are slower but may provide otherwise a similarly good account of blood volume[41].

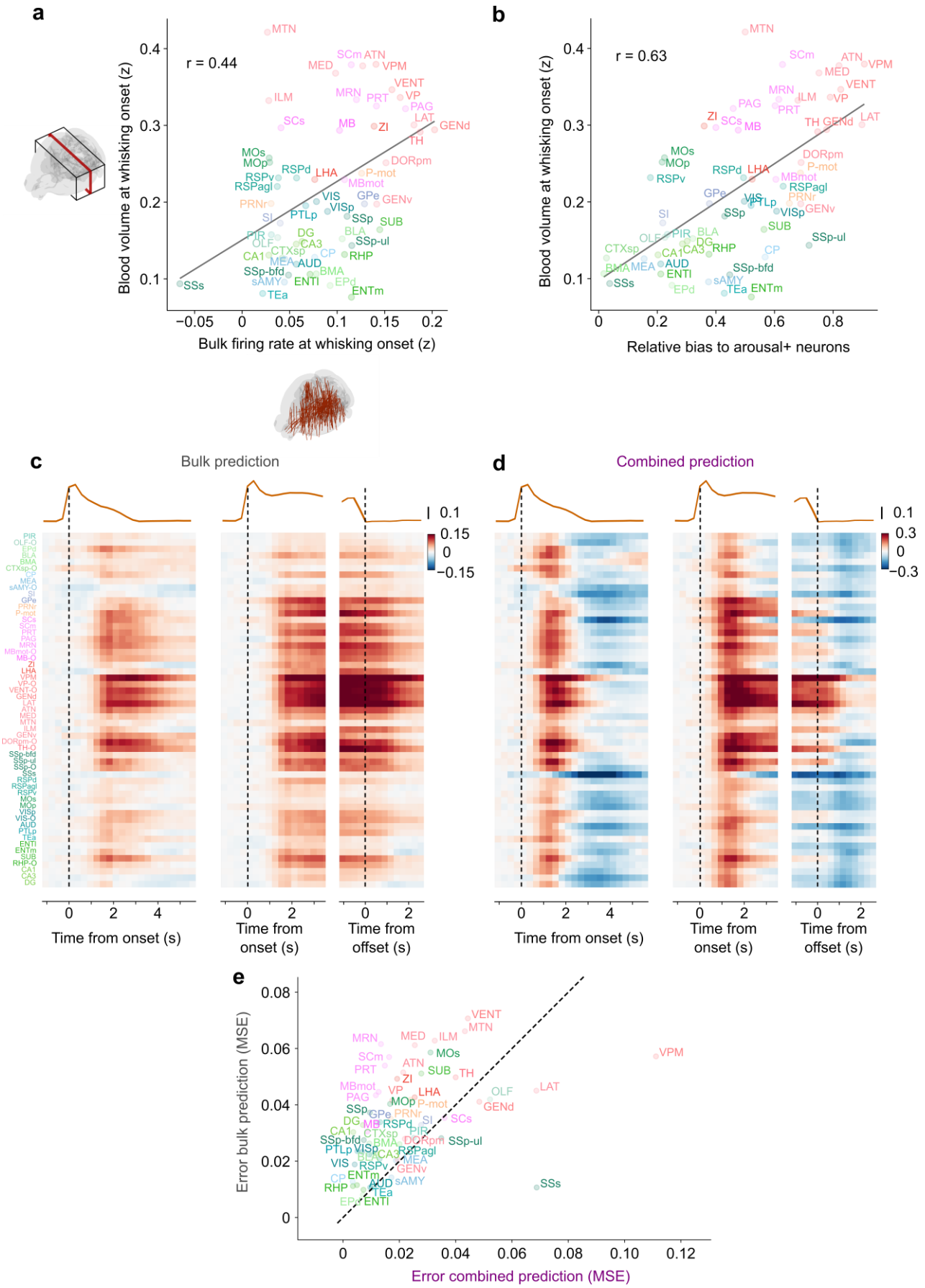

Figure 5. **The two arousal–based populations better predict brainwide blood volume around arousal events. a**. Average blood volume (from the brainwide fUSI recordings) 1.2-1.8 s after whisking onset plotted against average bulk firing rate (from

the brainwide Neuropixels recordings) 0-0.6 s after whisking onset. Each dot is a brain region, accompanied by its Allen acronym. The line shows a linear fit and r indicates the Pearson correlation. **b**. Same as **a**, comparing blood volume to the relative bias to arousal+ vs. arousal– neurons (computed as the difference in the number of arousal+ and arousal– neurons over their sum). **c.** Bulk prediction of whisking-evoked changes in blood volume, obtained by convolving whisking-related bulk firing rate (as shown in Figure 4Figure S8) with the filter from Figure 2e, averaged between visual cortex and hippocampus (Figure S4). **d.** Combined prediction of whisking-related blood volume from arousal+ neurons and arousal– neurons, obtained by convolving the firing rate of the two populations (as shown in Figure 4d, e) with their respective filters from Figure 3e, averaged between visual cortex and hippocampus (Figure S4) and summing their contributions scaled by the proportion of arousal+ and arousal- neurons in each region. **e**. Mean squared error (MSE) between actual and predicted whisking-related blood volume for the bulk prediction, plotted against the MSE for the combined prediction. The MSE is computed across time for the brief and longer whisking bouts (0-4.5 s window). Each dot is a brain region, accompanied by its Allen acronym.

Fluctuations in blood volume, however, were better explained by the activity and relative abundance of arousal+ and arousal– in each brain region. This relative abundance varied substantially across regions. This variation may explain why some cortical regions have been found to be positively vs. negatively correlated with locomotion[34,47-49]. Indeed, the abundance of arousal– neurons in auditory cortex is consistent with the high numbers of neurons suppressed by locomotion in that region[50].

Once the diverse abundance of the two populations is taken into account, neurovascular coupling is consistent across brain regions. Our results thus may reconcile two views of neurovascular coupling: that it is consistent[10,19,20] vs. diverse[5,13,15-18] across regions. Perhaps studies that found it to be consistent compared regions with similar fractions of arousal+ and arousal– neurons, and studies that found it to be variable compared regions with different fractions.

Our results also support the view that neurovascular coupling is consistent across brain states. Indeed, we found that the activity of the two opposing populations could predict blood volume across arousal states ranging from quiet periods — which likely included sleep — to long whisking bouts. This result contradicts previous studies that found neurovascular coupling to differ across brain states[5,20-22]. However, these studies used bulk measures of neural activity, so they could not distinguish the state-dependent contributions of arousal+ and arousal– neurons.

The ability of the two opposing populations to predict blood volume may be even higher than it appears from our analyses. Indeed, our analyses relied on three datasets obtained in different mice, laboratories, and conditions. This uncontrolled variation is likely to affect mouse behavior, making the comparison more difficult. For instance, the mice were likely quietest in the simultaneous fUSI and Neuropixels recordings, which were performed in long sessions with no task. By contrast, the brainwide Neuropixels recordings that we analyzed were briefer and performed right after the mouse performed a task.

Moreover, the relationship between neural activity and blood volume may have higher dimensionality. We have distinguished two populations of neurons, arousal+ and arousal–, based on their correlation with whisking. There may be other ways to distinguish the activity of neurons that would lead to even better predictions. These improved approaches might identify more than two subpopulations, each with their own HRF.

The relationship between the blood supply and the activity of the two opposing populations is likely to be at least partly causal. The simplest explanation is that the arousal+ and arousal– populations are each related to blood volume through their own distinct neurovascular coupling mechanisms. In this view, the relationship between activity and blood volume would be entirely causal. Alternatively, there could be an additional direct link between the factors that control the activity of those two populations and blood volume. These factors have been studied extensively in the cortex and in thalamus, and include neuromodulation[39,51-55] and inhibition[34,56-60]. These factors may affect different populations of neurons differently. Our data do not distinguish between these explanations. They do, however, reveal that neurovascular coupling is different in two key neural populations with opposite relation to arousal.

Supplementary materials

Piriform area	CH	CTX	CTXpl	OLF	PIR		
Cortical amygdalar area posterior part	CH	CTX	CTXpl	OLF	COA	COAp	
Olfactory areas - other	CH	CTX	CTXpl	OLF-O			
Endopiriform nucleus, dorsal part	CH	CTX	CTXsp	EP	EPd		
Basolateral amygdalar nucleus	CH	CTX	CTXsp	BLA			
Basomedial amygdalar nucleus	CH	CTX	CTXsp	BMA			
Cortical subplate - other	CH	CTX	CTXsp-O				
Caudoputamen	CH	CNU	STR	STRd	CP		
Medial amygdalar nucleus	CH	CNU	STR	sAMY	MEA		
Striatum-like amygdalar nuclei - other	CH	CNU	STR	sAMY-O			
Substantia innominata	CH	CNU	PAL	PALv	SI		
Globus pallidus, external segment	CH	CNU	PAL	PALd	GPe		
Pallidum dorsal region - other	CH	CNU	PAL	PALd-O			
Pontine reticular nucleus	BS	HB	P	P-sat	PRNr		
Pons, motor related	BS	HB	P	P-mot			
Substantia nigra, reticular part	BS	MB	MBmot	SNr			
Superior colliculus, motor related	BS	MB	MBmot	SCm			
Superior colliculus, sensory related	BS	MB	MBsen	SCs			
Pretectal region	BS	MB	MBmot	PRT			
Periaqueductal gray	BS	MB	MBmot	PAG			
Midbrain reticular nucleus	BS	MB	MBmot	MRN			
Midbrain motor related - other	BS	MB	MBmot-O				
Midbrain - other	BS	MB-O					
Mammillary body	BS	IB	HY	MEZ	MBO		
Hypothalamic medial zone - other	BS	IB	HY	MEZ-O			
Zona incerta	BS	IB	HY	LZ	ZI		
Lateral hypothalamic area	BS	IB	HY	LZ	LHA		
Hypothalamic lateral zone - other	BS	IB	HY	LZ-O			
Periventricular zone	BS	IB	HY	PVZ			
Periventricular region	BS	IB	HY	PVR			
Ventral posteromedial nucleus of the thalamus	BS	IB	TH	DORsm	VENT	VP	VPM
Ventral posteromedial complex - other	BS	IB	TH	DORsm	VENT	VP-O	
Ventral group of the dorsal thalamus - other	BS	IB	TH	DORsm	VENT-O		
Geniculate group, dorsal thalamus	BS	IB	TH	DORsm	GENd		
Thalamus, sensory-motor cortex related - other	BS	IB	TH	DORsm-O			
Lateral group of the dorsal thalamus	BS	IB	TH	DORpm	LAT		
Anterior group of the dorsal thalamus	BS	IB	TH	DORpm	ATN		
Medial group of the dorsal thalamus	BS	IB	TH	DORpm	MED		
Midline group of the dorsal thalamus	BS	IB	TH	DORpm	MTN		
Intralaminar nuclei of the dorsal thalamus	BS	IB	TH	DORpm	ILM		
Geniculate group, ventral thalamus	BS	IB	TH	DORpm	GENv		
Epithalamus	BS	IB	TH	DORpm	EPI		
Thalamus, polymodal cortex related - other	BS	IB	TH	DORpm-O			
Thalamus - other	BS	IB	TH-O				
Primary somatosensory area, nose	CH	CTX	CTXpl	Isocortex	SS	SSp	SSP-n
Primary somatosensory area, barrel field	CH	CTX	CTXpl	Isocortex	SS	SSp	SSP-bfd
Primary somatosensory area, lower limb	CH	CTX	CTXpl	Isocortex	SS	SSp	SSP-ll
Primary somatosensory area, upper limb	CH	CTX	CTXpl	Isocortex	SS	SSp	SSP-ul
Primary somatosensory area - other	CH	CTX	CTXpl	Isocortex	SS	SSp-O	
Supplemental somatosensory area	CH	CTX	CTXpl	Isocortex	SS	SSs	
Retrosplenial area, dorsal part	CH	CTX	CTXpl	Isocortex	RSP	RSPd	
Retrosplenial area, lateral agranular part	CH	CTX	CTXpl	Isocortex	RSP	RSPagl	
Retrosplenial area, ventral part	CH	CTX	CTXpl	Isocortex	RSP	RSPv	
Secondary motor area	CH	CTX	CTXpl	Isocortex	MO	MOs	
Primary motor area	CH	CTX	CTXpl	Isocortex	MO	MOp	
Primary visual area	CH	CTX	CTXpl	Isocortex	VIS	VISp	
Visual areas - other	CH	CTX	CTXpl	Isocortex	VIS-O		
Auditory areas	CH	CTX	CTXpl	Isocortex	AUD		
Posterior parietal association areas	CH	CTX	CTXpl	Isocortex	PTLp		

Temporal association areas	CH	CTX	CTXpl	Isocortex	**TEa**		
Entorhinal area, lateral part	CH	CTX	CTXpl	HPF	RHP	ENT	**ENTl**
Entorhinal area, medial part dorsal zone	CH	CTX	CTXpl	HPF	RHP	ENT	**ENTm**
Subiculum	CH	CTX	CTXpl	HPF	RHP	**SUB**	
Retrohippocampal region – other	CH	CTX	CTXpl	HPF	**RHP-O**		
Field CA1	CH	CTX	CTXpl	HPF	HIP	CA	**CA1**
Field CA3	CH	CTX	CTXpl	HPF	HIP	CA	**CA3**
Dentate gyrus	CH	CTX	CTXpl	HPF	HIP	**DG**	

Table S1: Names and acronyms of brain regions used in this study. Each row corresponds to a brain region, with its name and acronym written in color. Parent regions are indicated in black. Columns indicate hierarchical level as defined by the Allen Brain atlas (*left* to *right:* coarser to finer). Acronyms followed by -O (for 'Other') correspond to the described region excluding its child regions which are also brain regions considered in the study.

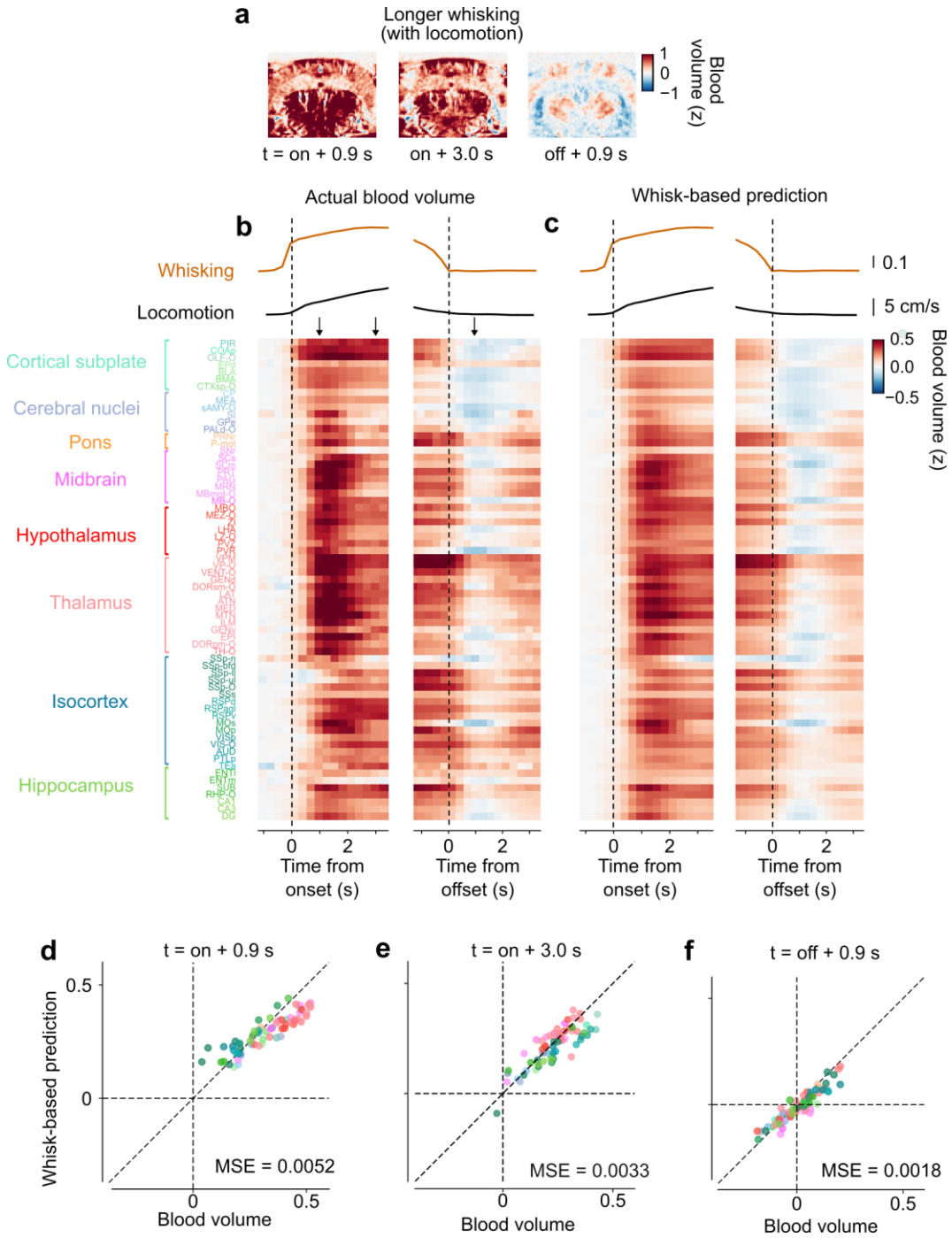

Figure S1. **Bouts of whisking accompanied by locomotion. a**. Average blood volume for long whisking bouts (> 3.5 s) accompanied by locomotion, 0.9 and 3.0 s after whisking onset, and 0.9 s after whisking offset, for the same example session as in Figure 1b-f. Each voxel is baseline-subtracted using a window of 0.5-2 s before whisking onset. **b.** Average changes in blood volume throughout all imaged regions during long whisking bouts accompanied by locomotion (> 3.5 s, average = 26.6 s), aligned to bout onset (*left*) and offset (*right*). Arrows indicate the times of the images in **a** and the quantifications in **d-f.** Colors indicate z-scored blood volume. **c.** Same, for predictions of blood volume from whisking (as in Figure S3). **d-e.** Comparison of predicted and actual blood volume 0.9 s (**d**) and 3.0 s (**e**) after the onset of long whisking bouts accompanied by locomotion. The mean squared error (MSE) between predicted and measured values across regions is indicated. Each dot is a brain region, colored as in **b**. **f.** Same as **d**, 0.9 s after whisking offset.

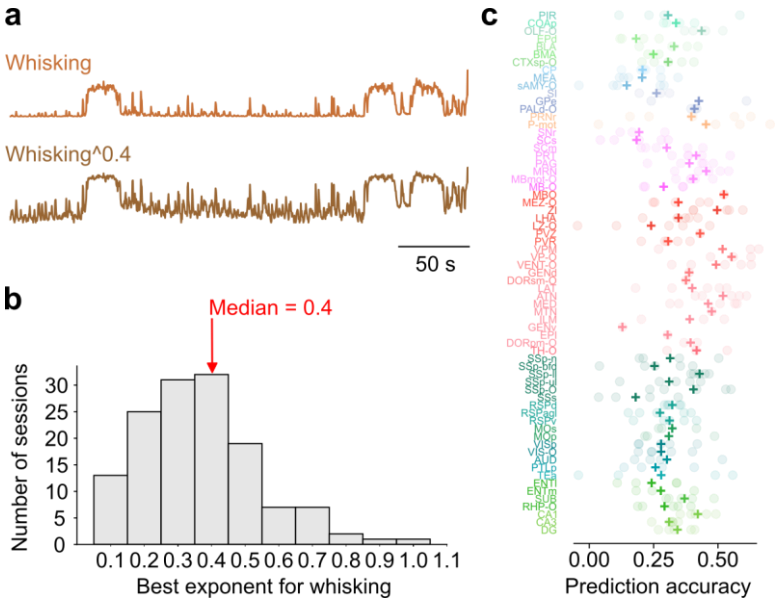

Figure S2. **Prediction of blood volume by whisking.** For each region, we used linear regression to obtain filters that predict that region's blood volume from whisking. **a.** We use exponentiated versions of whisking, with exponents ranging from 0.1 to 1.2 in 0.1 steps. Exponents < 1, like in this example, boost small fluctuations in whisking relative to larger whisking events (which are typically associated with locomotion). For each session, we use the best exponent for that session. **b.** Histogram of best values of exponents applied to whisking (which led to highest prediction accuracy), across all sessions. **c.** Median prediction accuracy, computed as the Pearson correlation across time between actual blood volume and cross-validated predictions, averaged across sessions for each brain region. Each dot corresponds to a mouse, and the cross indicates the mean across animals.

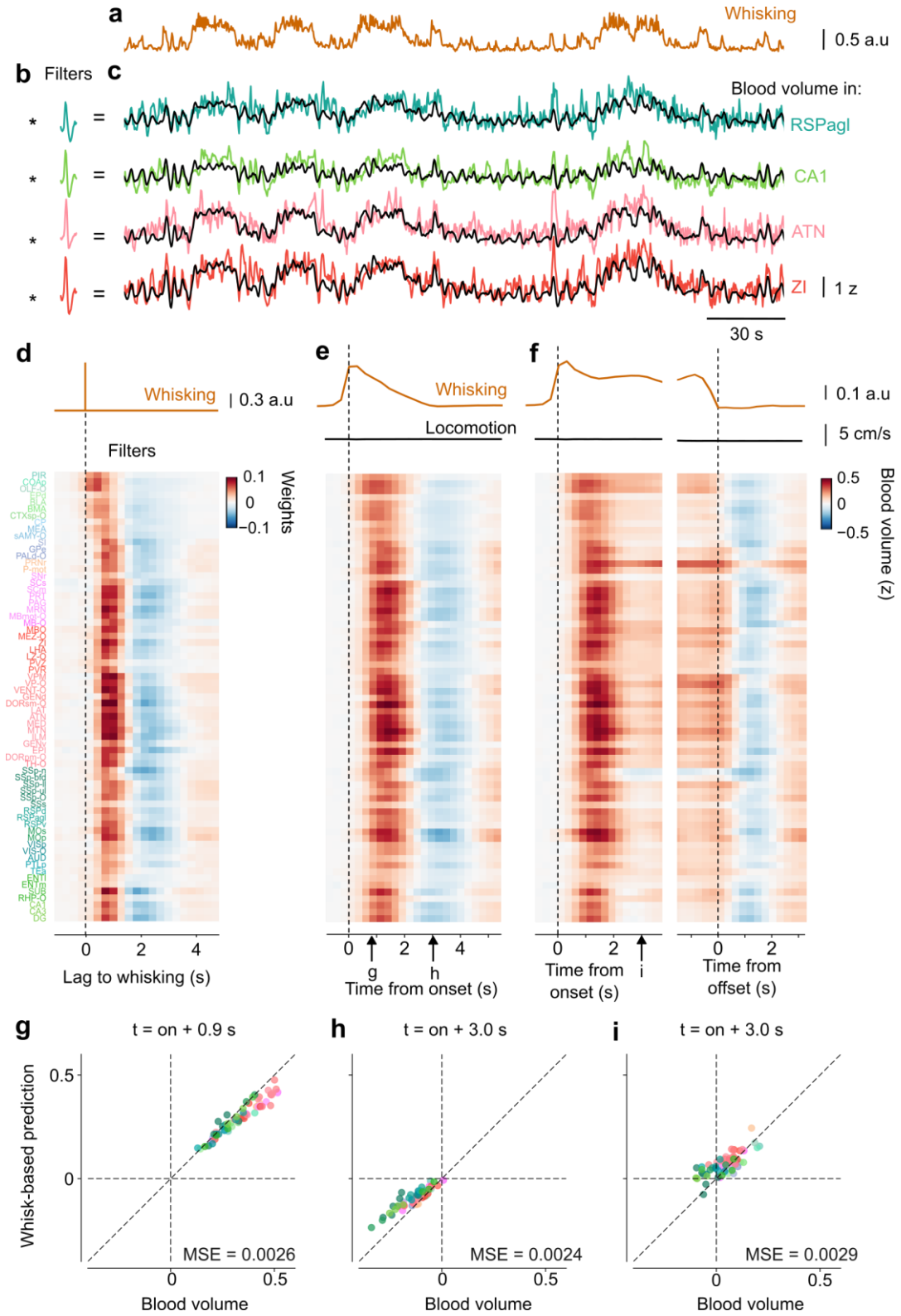

Figure S3. **Whisking predicts brainwide blood volume throughout arousal events. a.** For each region, we used linear regression to obtain filters that predict that region's blood volume from whisking. These predictions were improved by applying a compressive nonlinearity to the whisking traces, which boosted small whisking events (Figure S2). **b**. Best-fitting filters to predict blood volume from whisking, in the 4 example brain regions shown in Figure 1. **c.** Blood volume measured in those 4 regions (*colored curves*), and predictions obtained by filtering the whisking trace in a with the filters in **b** (*black curves*). **d**. Best-fitting filters obtained for all brain regions, which model changes in blood volume for a Dirac delta function of whisking. **e-f**. Predicted blood volume fluctuations throughout all brain regions, for brief and longer whisking bouts without locomotion. Format as in Figure 1**g-h**. **g-h**. Comparison of predicted and actual blood volume for the briefer whisking events in e, 0.9 s (**g**) and 3.0 s (**h**)

after whisking onset. Values of the mean squared error (MSE) between predicted and measured values across regions are indicated. Each dot is a brain region, colored as in **d**. **i.** Same as **h**, for the longer bouts in **f**.

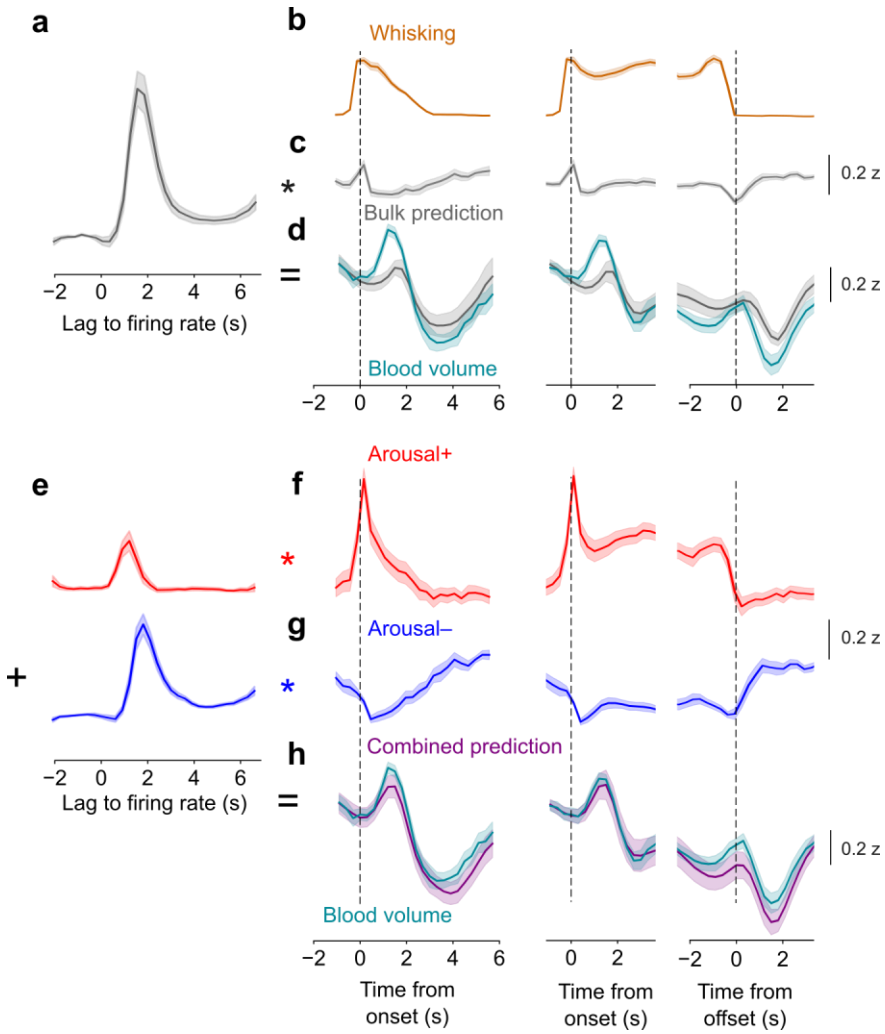

Figure S4. **Predicting blood volume from firing rate of different populations for recordings in hippocampus. a**. The best-fitting filter to predict blood volume from average firing rate. **b.** We identified whisking bouts and looked at brief (left) and longer whisking bouts, aligned to onset (middle) or offset (right). **c**. Average changes in bulk firing rate during whisking events. **d**. Average change in blood volume during whisking events (*cyan*), and prediction from bulk firing rate (*grey*). **e**. The best-fitting filter to predict blood volume from arousal+ and arousal– neurons. **f**. Average changes in firing rate for arousal+ neurons during whisking events. **g**. Same, for arousal– neurons. **h.** Average change in blood volume during whisking events (*cyan*), and prediction from arousal+ and arousal– neurons (*purple*).

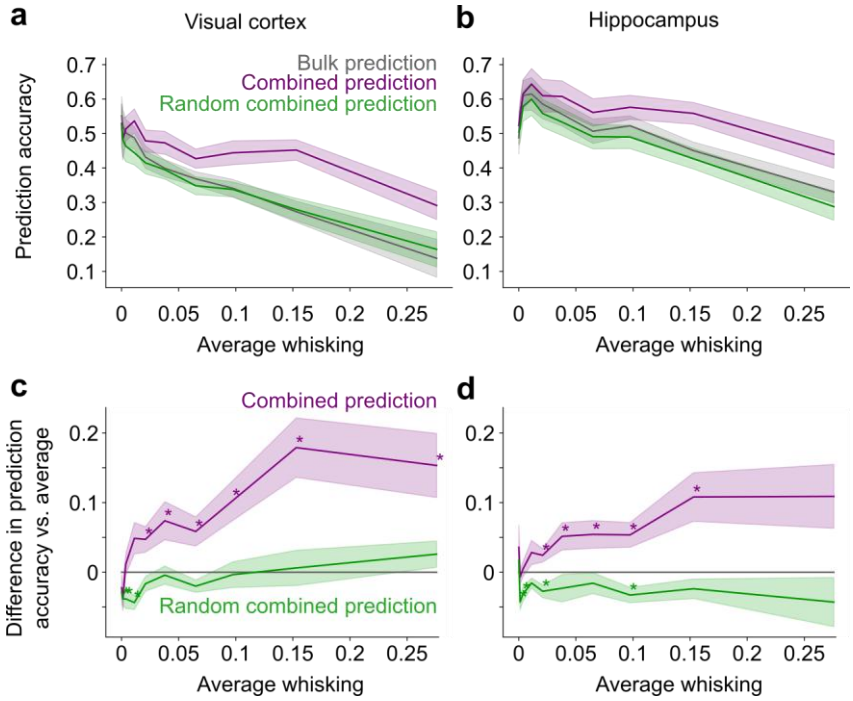

Figure S5. **Accuracy in predicting blood volume from firing rate across levels of arousal.** We cut each recording session into chunks of 10 s and computed the Pearson correlation between actual and predicted blood volume, as well as the average whisking within each chunk. We then binned chunks based on their average whisking and computed the median prediction accuracy within each bin of whisking. **a**. Average prediction accuracy across recording sessions, for the bulk prediction (*grey*), the combined prediction (*purple*), and the random combined prediction (*green*, see Figure S6) as a function of whisking bin, in visual cortex. **b**. Same as **a**, in hippocampus. **c**. Difference in prediction accuracy between the combined (*purple*), or random combined (*green*) and the bulk prediction, as a function of whisking bin, in visual cortex. Asterisks (*) indicate a significant difference ($p < 0.05$, paired t-test across recording sessions). **d**. Same as **c**, in hippocampus.

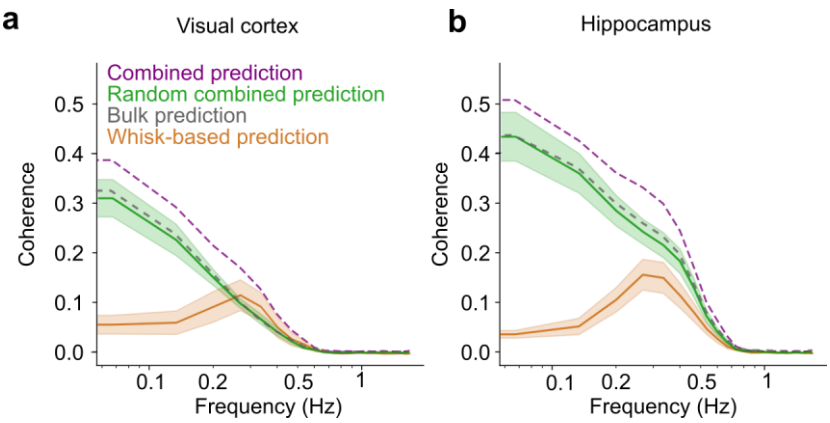

Figure S6. **Prediction of blood volume from two random populations. a**. To assess the importance of arousal+ and arousal– populations, we computed predictions of blood volume in visual cortex by fitting filters for the average firing rate of two random populations of neurons, matched in size with arousal+ and arousal– populations (random combined prediction, *green*). This prediction led to a coherence with true blood signal similar and slightly worse than the bulk prediction (*dashed grey*, p = 0.07 across frequencies), and worse than the combined prediction (*dashed purple,* p = 1e-3). Predictions from whisking alone (*gold*) were also worse than the combined prediction (p = 0.02). Shaded areas correspond to +/- one standard error. **b**. The same results were found in hippocampus: the predictions from the two random populations were similar to those from bulk firing rate (p = 0.18), and worse than the combined prediction (p = 4e-4), as for the prediction from whisking alone (p = 8e-5).

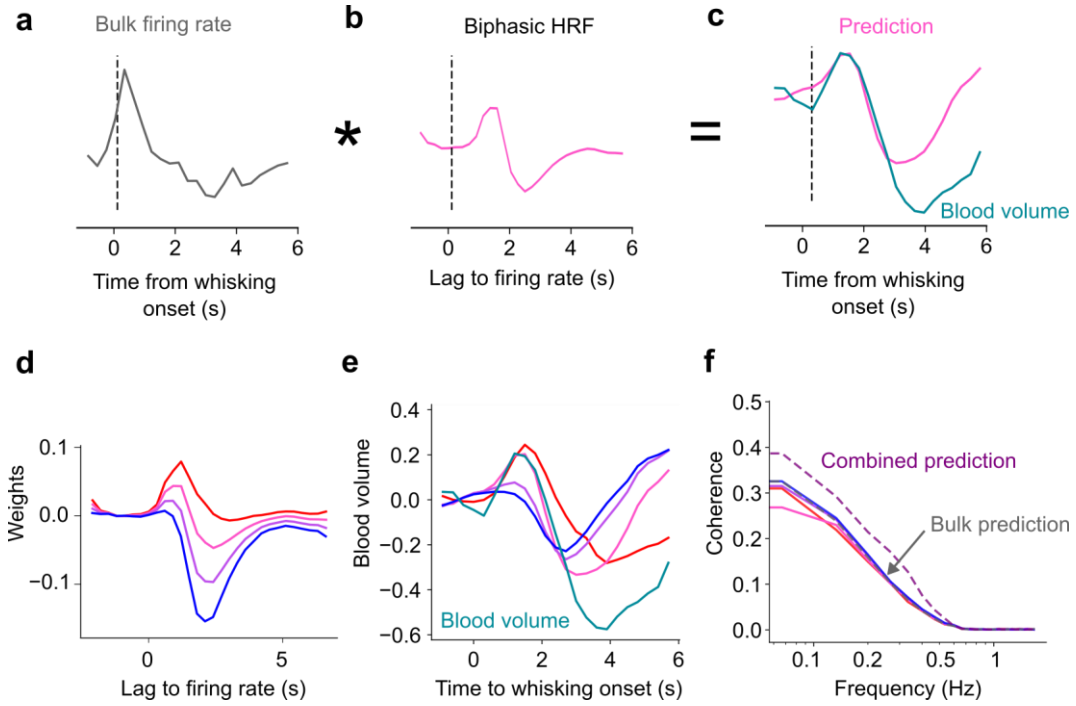

Figure S7. **Prediction of blood volume from average firing rate with biphasic filters**. We tested whether a biphasic filter on average firing rate could also reach the results we obtained with the combined prediction. We convolved bulk firing rate (**a**) with a biphasic filter (**b**) obtained by taking a weighted difference between the obtained filter for arousal+ neurons and the filter for arousal– neurons. We then aligned the obtained predictions to whisking onsets and compared them to actual blood volume (**c**). **d.** We used this procedure with different relative weights between arousal+ and arousal– filters. **e.** None of these filters recapitulated the dynamics seen in blood volume (*cyan*) following whisking events. Some produced biphasic responses but with a different timescale and amplitude. **f.** Coherence between actual and predicted blood volume for the different filters. All the predictions obtained through this procedure were significantly worse than the combined prediction (*dashed purple*, $p < 0.02$ in visual cortex, shown here, $p < 2e\text{-}3$ in hippocampus), and similar or worse than the bulk prediction (*dashed grey,* $p = 0.04\text{-}0.78$ in visual cortex, $p = 3e\text{-}3 – 0.34$ in hippocampus).

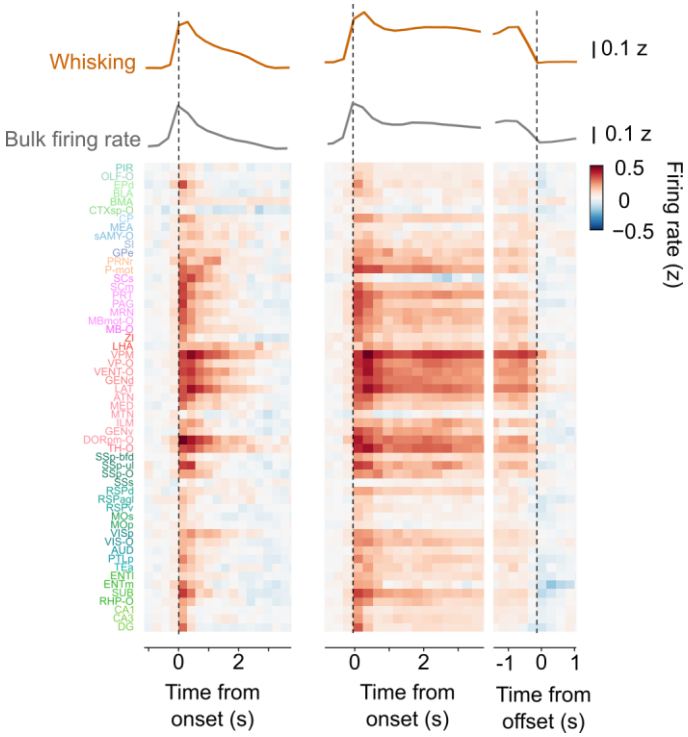

Figure S8**. Average firing rate during whisking events.** Average firing rate during brief whisking events (*left*), longer whisking events, aligned to onset (*middle*) or offset *(right*), for all regions. The grey trace indicates the average across all regions.

Acknowledgments

We thank Charu Reddy for invaluable help with surgeries and lab management. This work was supported by the Wellcome Trust (grant 223144/Z/21/Z to MC and KDH) and the US BRAIN initiative (NIH grant U19NS123716 to the International Brain Laboratory). MC holds the GlaxoSmithKline / Fight for Sight Chair in Visual Neuroscience.

Methods

Brainwide fUSI measurements

Experiments were conducted in 5 C57/BL6 mice (3 male, 2 female), 13-34 weeks of age. All experimental procedures were conducted according to the UK Animals Scientific Procedures Act (1986). Experiments were performed at University College London, under a Project License released by the Home Office following appropriate ethics review.

Surgery

Mice were first implanted with a headplate and cranial window under surgical anesthesia in sterile conditions. The cranial window replaced a dorsal section of the skull (~8 mm in ML and ~5 mm in AP) with 90 µm thick ultrasound-permeable polymethylpentene (PMP) film (TPX DX845 PMP, Goodfellow Cambridge Ltd.) attached to the skull with cyanoacrylate glue. The PMP film was then covered with Kwik-Cast (World Precision Instruments, USA), except during imaging sessions. After surgery, mice were allowed to recover for 7 days before starting habituation. Mice were then habituated to handling and head-fixation in the rig across several days, as session duration progressively increased.

Histology

Mice were perfused with PBS, PFA, and a gel containing TRITC–Dextran (Sigma-Aldrich) to perform blood vessel labelling. We imaged full 3D stacks of the brains in a custom-made serial section [61] two-photon[62] tomography microscope. Images were acquired using ScanImage (Vidrio Technologies) and the hardware coordinated using BakingTray. We extracted the signal in green and red channels, for autofluorescence and labelled blood vessels.

fUSI recording sessions

Recordings were performed in 5 mice across different days for up to 10 weeks. On a given day, we sequentially recorded 2-3 sessions in different coronal planes, lasting ~45 min each. The final dataset consisted of 138 such sessions for a total of 101 hours of recordings, ranging from 17 to 24 hours per mouse.

In each recording session, we head-fixed the mice by securing the headplate to a post placed 10 cm from three video displays (Adafruit, LP097QX1, 60 Hz refresh rate) arranged at right angles to span 270 deg in azimuth and ~70 deg in elevation. The screens were uniform gray or black. In some sessions (13 out of 138), the screens switched from gray to black, or from black to gray halfway through the recording session. The mice were placed on a running wheel. Four infrared cameras and the wheel rotary encoder were used to monitor their spontaneous behavior.

We covered the PMP film with ultrasound gel and positioned an ultrasound transducer above it (128-element linear array, 100 µm pitch, 8 mm focal length, 15 MHz central frequency, model L22-Xtech, Vermon, France). Doppler signals from the transducer were acquired using an ultrasound system (Vantage 128, Verasonics, USA) controlled by a custom Matlab-based user interface (Alan Urban Consulting) recording continuously at 500 Hz.

fUSI preprocessing and denoising

Coherent tissue motion was removed by performing SVD on the complex images (IQ data) in overlapping 600 ms windows (300 ms overlap) and discarding the first 50 principal components[63]. Power doppler images were then obtained by computing the average squared

modulus of the filtered IQ data over non-overlapping 300 ms windows.

Power doppler data was further denoised using several steps:

1. To correct brain deformation across multiple voxels, we performed motion registration. We used NoRMCorre, a piecewise-rigid registration algorithm from CaImAn[64].
2. To correct for timepoints with artifactually high values (outliers), we ran a procedure to identify those and replaced them through linear interpolation of neighboring frames.
   The detection was based on (a) identifying noisy voxels as those with kurtosis across time above 10, (b) computing the changes between successive frames of the average activity of these noisy voxels, (c) identifying time points in which this signal was greater than the mean by 3 standard deviations.
3. To correct for residual contamination of movement artefacts, we removed any activity that could be linearly predicted from out-of-brain voxels (mostly located in the ultrasound gel, above the surface of the brain). We identified out-of-brain voxels based on low average activity and not being assigned to any brain region. We computed SVD on out-of-brain voxel activity and used the first 5 components as regressors. We fitted linear weights to predict the full power doppler using ridge regression and subtracted this prediction from the data.

We then z-scored the activity of each voxel across time.

Alignment to Allen atlas and region extraction

To extract signals for different brain regions and combine data across sessions and animals, we used a custom, individual-based alignment to the Allen Common Coordinate Framework atlas (CCF, [38]).

For each animal, we ran an anatomical scan using a motor interface. This scan consisted of average Power Doppler images for short fUSI acquisitions in slices 0.1 mm apart, covering the whole craniotomy. This served as a reference to which we aligned each individual session, as well as the histology.

We perfused each animal using a blood vessel labelling procedure and imaged the brain (see Histology), extracting signals in two color channels: green for autofluorescence and red for labelled blood vessels. We aligned the volume to the Allen CCF atlas using the autofluorescence channel with brainreg[65-67].

We then aligned the in-vivo fUSI anatomical scan of each animal to its in-vitro volume using the stained blood vessels. To do so, we used an affine transformation fit to minimize the distance between several manually identified matched keypoints (~15-30) in both volumes. These were typically branching between big blood vessels visible in both the in-vivo, lower resolution fUSI scan, and the in-vitro, higher resolution histology volume. We visually confirmed the proper alignment between the two volumes and then transposed the Allen regions labels to our fUSI volume, so that we obtained a region label for each voxel of the scan.

To select the target regions to keep for our analyses, we first mapped the region labels to the coarser Beryl mapping[36]. Some of these regions were too small to be identified with confidence with the resolution of fUSI. Thus, we set a threshold of volume for regions to be considered (~0.8 mm^3). We then assigned regions smaller than this threshold to their parent region and reiterated the procedure until all regions reached the threshold. This procedure resulted in the co-existence of regions at various stages of hierarchy, for example VPM, VP and VENT. To clarify that these excluded some regions, we used the -O to indicate "other", in VP-O and VENT-O. A full list of region names and acronyms is shown in Table S1.

To account for the off-plane (AP) spatial resolution of fUSI (~0.4 mm), we then computed the mode region label of each voxel across the AP axis in a 0.4 mm range. We only assigned a region to a voxel if the mode corresponded to more than 2/3 of the values. Thus, voxels in zones of transitions between different regions were not assigned to any region.

For each recording session, we then aligned the slice to our reference anatomical scan in two steps: (a) manual assignment to the closest AP slice in the reference scan, (b) cross-correlation in space with the chosen slice of the reference scan. We then used the region labels from the aligned reference scan.

We discarded voxels with very little signal due to shadowing, for e.g. due to bone regrowth. To do so, we applied a Sobel filter to the anatomical image, which computes an approximation of the gradient of the intensity of the image, or edges. We identified shadowed areas by patches of the image (> 30 voxels) with consistently low values of the Sobel filtered image. Indeed, in the brain, individual vessels create a lot of edges, so that big patches of low values only occur outside of the brain, or when vessels are hidden by bone.

Once we obtained region labels for each recorded voxel, we computed the region signal for this session using the median activity across voxels. For each recording session, we only considered regions with more than 20 voxels in the slice. Region signals were extracted for each hemisphere separately and then averaged across the two hemispheres. For further analysis, we considered all regions for which we recorded at least 10 sessions in total over all animals.

Behavior analysis and extraction of onsets

Locomotion velocity was obtained from the rotary encoder.

Whisking measurements were obtained through Facemap[30]. Whisking was obtained by taking the first component of a SVD decomposition of motion energy over the whisker pad. This was done on either one or two cameras (corresponding to both sides of the mouse face). If the signal was available for two cameras, we used the average across both cameras. To have a comparable signal across sessions, we ensured that higher values corresponded to higher motion, and normalized the signal between 0 and 1, based on the 1st percentile and the maximum.

All behavioral metrics were binned in the same 300 ms bins as the fUSI data.

Whisking bouts were detected when the signal crossed a given threshold (0.15) and lasted until the signal reached another threshold (0.05) under the condition that the average whisking in the next 4 s remained below this threshold (this is to exclude very short interruptions in longer whisking bouts and allow better separation of whisking bouts).

Brief bouts were defined as bouts with duration between 1.3 and 3.5 s, while longer bouts lasted longer than 3.5 s. Whisking bouts were considered accompanied by locomotion when wheel velocity above 1 cm/s was detected at any point in the 6 seconds following whisking onset.

For all plots of changes in activity (blood volume, firing rate) associated with whisking events, we followed the following procedure. We first aligned data to the detected onsets (or offsets) and averaged across the bouts of interest. Before averaging, for each bout we excluded times when another, following whisking bout had started. We then recentered by the baseline activity (0.5-2 s before whisking onset).

Predictions from whisking

To predict blood volume from whisking, we used cross-validated ridge regression. The lambda hyperparameter used for regularization was fitted through nested cross-validation. A feature matrix was constructed using lagged versions of the whisking trace, with lags ranging from -1.8 to 5.7 s (positive lags mean that whisking precedes blood volume). This was used to predict activity in each brain region, for each session. For each session, we allowed for a different non-linear scaling of whisking (the same across all regions). We ran predictions from whisking raised to the power of different values (from 0.1 to 1.2 with steps of 0.1) and selected the value providing the best prediction accuracy (averaged across regions). The median exponent across sessions was 0.4, so that this procedure gave more relative weight to small whisking events relative to the strong whisking associated for example with locomotion (Figure S2).

Combined fUSI and Neuropixels recordings

For combined fUSI and neuronal recordings, we used our published dataset[10] which combines Neuropixels recordings in visual cortex and hippocampus with fUSI at the same planes, in 5 C57/BL6 mice (4 male, 1 female), 9-12 weeks of age (see Ref[10] for details). We used all recording times, including visual stimulation and spontaneous activity.

Power Doppler was recomputed from IQ data to match the pre-processing steps explained above. Blood volume, whisking and single-unit firing rate were all binned in 300 ms bins. Units selected were 'good clusters' from Kilosort as in Ref. [10]. Blood volume was averaged within two regions of interest, corresponding to voxels immediately around the probe track and in either visual cortex or hippocampus (~50 voxels in each region), bilaterally when available.

We computed the Pearson correlation with whisking in two splits of the session. We defined neurons as 'arousal+' if this correlation was above 0.05 on both splits of the data, and 'arousal–' if it was below -0.05 on both splits. We first z-scored the firing rate of each neuron throughout the session and then averaged these across neurons of each group (arousal+, arousal–, or all).

For the example session in Figure 3b-d, we computed the correlation of neurons with whisking and defined arousal+ and arousal– neurons on half of the session (split 1). Figure 3b is ordered by the correlation with whisking on split 1 but shows a snippet of the other half of the recording session (split 2).

We fit filters to predict blood volume from the average firing rate(s) of either all neurons, or arousal+ and arousal– neurons using linear regression with Lasso regularization, for each region and session separately. We used lags ranging from -2.1 s to 6.6 s in 0.3 s intervals, where positive lags mean that firing rate precedes blood volume. Cross-validation was done using folds of ~8 min, with nested cross-validation for the regularization hyperparameter. The definition of arousal+ and arousal– neurons was done on the whole recording session and not included in the cross-validation loop.

Actual and predicted traces of blood volume were z-scored throughout the session before alignment to whisking events.

To evaluate fit quality, we computed the coherence between actual and (cross-validated) predicted blood volume, which is like correlation in the frequency domain. Specifically, we estimated the magnitude squared coherence estimate using Welch's method with 15 s windows and 7.5 s overlap between windows. To compare different predictions, we ran paired t-tests between the average coherence between actual and predicted blood volume (for all frequency bands below 0.7 Hz) for pairs of predictions (n = 10 sessions per region).

We also fit filters to predict blood volume from two random populations of neurons, matched in size with arousal+ and arousal– neurons, as well as from whisking (Figure S6). In addition, we verified how prediction accuracy for different predictions varied as a function of behavioral state, inferred from whisking. We cut each recording session into chunks of 10 s and computed the Pearson correlation between actual and predicted blood volume, as well as the average whisking within each chunk. We then binned chunks based on their average whisking and computed the median prediction accuracy within each bin of whisking, for each recording session. Bins were defined as the deciles of the observed distribution of these chunk average whisking values across all recording sessions. We then computed the average prediction accuracy in each bin across recording sessions, for different types of predictions (Figure S5). We also computed the difference in accuracy between the combined or random combined and the bulk prediction, as a function of whisking bin. We tested significant differences in each bin using a paired t-test across recording sessions and reported p-values < 0.05.

Finally, we looked at predictions obtained by applying biphasic filters to the bulk firing rate (Figure S7). We tested four such filters, obtained by taking the weighted difference between the filter we obtained for arousal+ neurons (weight *k*) and the filter we obtained for arousal– neurons (weight *1-k*), for *k* taking the following values: 0, 0.33, 0.66, 1. This was done for each recording session using the filters obtained for this specific session.

Brainwide Neuropixels recordings

We used Neuropixels recordings in the mouse brain performed in our consortium of laboratories as detailed elsewhere[36]. In the present analysis we included all sessions in which both video recordings and passive periods were available (n = 324 sessions). We focused our analysis on good units (N = 18,791 neurons) recorded in the passive periods, which occurred after the mice had performed the task.

Whisking was measured as the motion energy in a region of interest focused on the whisker pad, averaged across 1 to 2 cameras, binned in 300 ms windows, and normalized as previously (between 1st percentile and maximum).

We mapped neurons recorded across different animals and sessions to similar brain regions as measured in fUSI. To do so, we started with each neuron's label in the fine-grained Allen CCF labels. We then sorted the target brain regions by hierarchical level, starting with the lowest. For a given region, we included all neurons belonging to descendants of a region except if they had been already included in another child region. For example, VENT could contain neurons belonging to the subregions of VL, VAL, but not VP, since the latter was also a target region of interest. This procedure aimed to mimic what had been done for fUSI voxels, as well as ensuring that each neuron only featured in one target region. We excluded from further analysis regions containing less than 50 neurons for which spikes were detected during the passive periods.

Spikes of each neuron were binned in the same 300 ms bins as whisking. For each neuron, we z-scored the firing rate of each neuron across time within its recording session, detected whisking events as previously and aligned this signal to the whisking events. For each type of event (brief or longer bouts), we only included neurons for which at least 5 bouts were detected.

We computed the Pearson correlation with whisking in two splits of the session. We defined neurons as 'arousal+' if this correlation was above 0.05, and 'arousal–' if below -0.05. To count the number of reliable arousal+ and arousal– neurons in each region, we only considered neurons meeting the criterion in two splits of the session. We also computed an index measuring the relative bias to arousal+ neurons (Figure 5b) in each region by taking the difference between the number of arousal+ and arousal- neurons over their sum.

To look at whisking-related firing rate, we classified neurons based on one split and computed whisking-related changes in the other split (Figure 4, Figure 5, Figure S8). All whisking-related changes are baseline-subtracted (for each region), using a window of 0.5-2 s before whisking onset.

Predictions of brainwide whisking-related blood volume

To predict changes in blood volume (measured in the brainwide fUSI experiments) from the firing of neurons (measured in the brainwide Neuropixels recordings), we used the HRFs found from the combined fUSI-Neuropixels recordings, averaged across visual cortex and hippocampus. We assigned a neuron to arousal+ or arousal– groups based on half of the recording session and used its average firing rate on whisking bouts on the other half of the session. For each region, we then averaged this cross-validated firing rate across all arousal+ or arousal– neurons and convolved it with their respective filters. We first rescaled the arousal+ filter by the ratio of the proportion of arousal+ neurons in this region to the average proportion of arousal+ neurons in the simultaneous fUSI-Neuropixels recordings (across hippocampus and visual cortex). We did the same for arousal– filters and summed the contributions

from both filters. For the predictions from bulk firing rate, we used the corresponding filter with the same scaling for all regions and used firing for the same half as for the other prediction. Finally, we applied a global scaling factor to each type of prediction (the same across all regions). This scaling factor was obtained by minimizing the mean squared error between the predicted and actual blood volume -1.2 to 5 s from whisking onset, for brief and long bouts, across all regions. We similarly computed the mean squared error for each region separately and compared those between the combined and bulk prediction (Figure 5e).

Visualization

The 3D brain visualizations were generated using Urchin.

References

1 Heeger, D. J. & Ress, D. What does fMRI tell us about neuronal activity? *Nat Rev Neurosci* **3**, 142-151 (2002). https://doi.org/10.1038/nrn730

2 Drew, P. J. Vascular and neural basis of the BOLD signal. *Current Opinion in Neurobiology* **58**, 61-69 (2019). https://doi.org/10.1016/j.conb.2019.06.004

3 Logothetis, N. K. & Wandell, B. A. Interpreting the BOLD signal. *Annu Rev Physiol* **66**, 735-769 (2004). https://doi.org/10.1146/annurev.physiol.66.082602.092845

4 Hillman, E. M. Coupling mechanism and significance of the BOLD signal: a status report. *Annu Rev Neurosci* **37**, 161-181 (2014). https://doi.org/10.1146/annurev-neuro-071013-014111

5 Drew, P. J. Neurovascular coupling: motive unknown. *Trends Neurosci* **45**, 809-819 (2022). https://doi.org/10.1016/j.tins.2022.08.004

6 Logothetis, N. K., Pauls, J., Augath, M., Trinath, T. & Oeltermann, A. Neurophysiological investigation of the basis of the fMRI signal. *Nature* **412**, 150-157 (2001). https://doi.org/10.1038/35084005

7 Devor, A. *et al.* Coupling of the cortical hemodynamic response to cortical and thalamic neuronal activity. *PNAS* **102**, 3822-3827 (2005). https://doi.org/10.1073/pnas.0407789102

8 Mukamel, R. *et al.* Coupling Between Neuronal Firing, Field Potentials, and fMRI in Human Auditory Cortex. *Science* **309**, 951-954 (2005). https://doi.org/10.1126/science.1110913

9 Shmuel, A., Augath, M., Oeltermann, A. & Logothetis, N. K. Negative functional MRI response correlates with decreases in neuronal activity in monkey visual area V1. *Nature Neuroscience* **9**, 569-577 (2006). https://doi.org/10.1038/nn1675

10 Nunez-Elizalde, A. O. *et al.* Neural correlates of blood flow measured by ultrasound. *Neuron* **110**, 1631-1640 e1634 (2022). https://doi.org/10.1016/j.neuron.2022.02.012

11 Sirotin, Y. B. & Das, A. Anticipatory haemodynamic signals in sensory cortex not predicted by local neuronal activity. *Nature* **457**, 475-479 (2009). https://doi.org/nature07664 [pii]

10.1038/nature07664

12 Turner, K. L., Gheres, K. W. & Drew, P. J. Relating Pupil Diameter and Blinking to Cortical Activity and Hemodynamics across Arousal States. *J Neurosci* **43**, 949-964 (2023). https://doi.org/10.1523/JNEUROSCI.1244-22.2022

13 Ekstrom, A. How and when the fMRI BOLD signal relates to underlying neural activity: the danger in dissociation. *Brain research reviews* **62**, 233-244 (2010). https://doi.org/10.1016/j.brainresrev.2009.12.004

14 Jukovskaya, N., Tiret, P., Lecoq, J. & Charpak, S. What does local functional hyperemia tell about local neuronal activation? *J Neurosci* **31**, 1579-1582 (2011). https://doi.org/10.1523/JNEUROSCI.3146-10.2011

15 Devonshire, I. M. *et al.* Neurovascular coupling is brain region-dependent. *Neuroimage* **59**, 1997-2006 (2012). https://doi.org/10.1016/j.neuroimage.2011.09.050

16 Huo, B. X., Smith, J. B. & Drew, P. J. Neurovascular coupling and decoupling in the cortex during voluntary locomotion. *J Neurosci* **34**, 10975-10981 (2014). https://doi.org/10.1523/JNEUROSCI.1369-14.2014

17 Devor, A. *et al.* Stimulus-induced changes in blood flow and 2-deoxyglucose uptake dissociate in ipsilateral somatosensory cortex. *J Neurosci* **28**, 14347-14357 (2008). https://doi.org/10.1523/JNEUROSCI.4307-08.2008

18 Shih, Y. Y. *et al.* A new scenario for negative functional magnetic resonance imaging signals: endogenous neurotransmission. *J Neurosci* **29**, 3036-3044 (2009). https://doi.org/10.1523/JNEUROSCI.3447-08.2009

19 Boorman, L. *et al.* Negative blood oxygen level dependence in the rat: a model for investigating the role of suppression in neurovascular coupling. *J Neurosci* **30**, 4285-4294 (2010). https://doi.org/10.1523/JNEUROSCI.6063-09.2010

20 Scholvinck, M. L., Maier, A., Ye, F. Q., Duyn, J. H. & Leopold, D. A. Neural basis of global resting-state fMRI activity. *Proc Natl Acad Sci U S A* **107**, 10238-10243 (2010). https://doi.org/10.1073/pnas.0913110107

21 Winder, A. T., Echagarruga, C., Zhang, Q. & Drew, P. J. Weak correlations between hemodynamic signals and ongoing neural activity during the resting state. *Nat Neurosci* **20**, 1761-1769 (2017). https://doi.org/10.1038/s41593-017-0007-y

22 Turner, K. L., Gheres, K. W., Proctor, E. A. & Drew, P. J. Neurovascular coupling and bilateral connectivity during NREM and REM sleep. *eLife* **9** (2020). https://doi.org/10.7554/eLife.62071

23 Boynton, G. M. Spikes, BOLD, attention, and awareness: a comparison of electrophysiological and fMRI signals in V1. *J Vis* **11**, 12 (2011). https://doi.org/10.1167/11.5.12

24 Cardoso, M. M., Sirotin, Y. B., Lima, B., Glushenkova, E. & Das, A. The neuroimaging signal is a linear sum of neurally distinct stimulus- and task-related components. *Nat Neurosci* **15**, 1298-1306 (2012). https://doi.org/10.1038/nn.3170

25 Nir, Y. *et al*. Coupling between neuronal firing rate, gamma LFP, and BOLD fMRI is related to interneuronal correlations. *Curr Biol* **17**, 1275-1285 (2007). https://doi.org/10.1016/j.cub.2007.06.066

26 Buzsaki, G., Kaila, K. & Raichle, M. Inhibition and brain work. *Neuron* **56**, 771-783 (2007). https://doi.org/10.1016/j.neuron.2007.11.008

27 Attwell, D. *et al*. Glial and neuronal control of brain blood flow. *Nature* **468**, 232-243 (2010). https://doi.org/10.1038/nature09613

28 Echagarruga, C. T., Gheres, K. W., Norwood, J. N. & Drew, P. J. nNOS-expressing interneurons control basal and behaviorally evoked arterial dilation in somatosensory cortex of mice. *eLife* **9** (2020). https://doi.org/10.7554/eLife.60533

29 Vo, T. T. *et al*. Parvalbumin interneuron activity drives fast inhibition-induced vasoconstriction followed by slow substance P-mediated vasodilation. *Proc Natl Acad Sci U S A* **120**, e2220777120 (2023). https://doi.org/10.1073/pnas.2220777120

30 Stringer, C. *et al*. Spontaneous behaviors drive multidimensional, brainwide activity. *Science* **364**, 255 (2019). https://doi.org/10.1126/science.aav7893

31 Musall, S., Kaufman, M. T., Juavinett, A. L., Gluf, S. & Churchland, A. K. Single-trial neural dynamics are dominated by richly varied movements. *Nat Neurosci* **22**, 1677-1686 (2019). https://doi.org/10.1038/s41593-019-0502-4

32 Drew, P. J., Winder, A. T. & Zhang, Q. Twitches, Blinks, and Fidgets: Important Generators of Ongoing Neural Activity. *Neuroscientist* **25**, 298-313 (2019). https://doi.org/10.1177/1073858418805427

33 Macé, E. *et al*. Functional ultrasound imaging of the brain. *Nat Methods* **8**, 662-664 (2011). https://doi.org/10.1038/nmeth.1641

34 Garcia-Junco-Clemente, P. *et al*. An inhibitory pull–push circuit in frontal cortex. *Nat Neurosci* **20**, 389-392 (2017). https://doi.org/10.1038/nn.4483

35 Brécier, A., Borel, M., Urbain, N. & Gentet, J. L. Vigilance and Behavioral State-Dependent Modulation of Cortical Neuronal Activity throughout the Sleep/Wake Cycle. *J Neurosci* **42**, 4852-4866 (2022). https://doi.org/10.1523/JNEUROSCI.1400-21.2022

36 International Brain Laboratory *et al*. A Brain-Wide Map of Neural Activity during Complex Behaviour. *bioRxiv*, 2023.2007.2004.547681 (2024). https://doi.org/10.1101/2023.07.04.547681

37 Jun, J. J. *et al*. Fully integrated silicon probes for high-density recording of neural activity. *Nature* **551**, 232-236 (2017). https://doi.org/10.1038/nature24636

38 Wang, Q. *et al*. The Allen Mouse Brain Common Coordinate Framework: A 3D Reference Atlas. *Cell* **181**, 936-953.e920 (2020). https://doi.org/10.1016/j.cell.2020.04.007

39 Collins, L., Francis, J., Emanuel, B. & McCormick, D. A. Cholinergic and noradrenergic axonal activity contains a behavioral-state signal that is coordinated across the dorsal cortex. *eLife* **12**, e81826 (2023). https://doi.org/10.7554/eLife.81826

40 McGinley, M. J. *et al*. Waking State: Rapid Variations Modulate Neural and Behavioral Responses. *Neuron* **87**, 1143-1161 (2015). https://doi.org/10.1016/j.neuron.2015.09.012

41 Pisauro, M. A., Benucci, A. & Carandini, M. Local and global contributions to hemodynamic activity in mouse cortex. *J Neurophysiol* **115**, 2931-2936 (2016). https://doi.org/10.1152/jn.00125.2016

42 Aydin, A.-K. *et al*. Transfer functions linking neural calcium to single voxel functional ultrasound signal. *Nat Comm* **11**, 2954 (2020). https://doi.org/10.1038/s41467-020-16774-9

43 Reimer, J. *et al*. Pupil Fluctuations Track Fast Switching of Cortical States during Quiet Wakefulness. *Neuron* **84**, 355-362 (2014). https://doi.org/10.1016/j.neuron.2014.09.033

44 Vinck, M., Batista-Brito, R., Knoblich, U. & Cardin, J. A. Arousal and locomotion make distinct contributions to cortical activity patterns and visual encoding. *Neuron* **86**, 740-754 (2015). https://doi.org/10.1016/j.neuron.2015.03.028

45 Reimer, J. *et al*. Pupil fluctuations track rapid changes in adrenergic and cholinergic activity in cortex. *Nat Commun* **7**, 13289 (2016). https://doi.org/10.1038/ncomms13289

46 Pais-Roldán, P. *et al*. Indexing brain state-dependent pupil dynamics with simultaneous fMRI and optical fiber calcium recording. *PNAS* **117**, 6875-6882 (2020). https://doi.org/10.1073/pnas.1909937117

47 Fisher, P. S. *et al*. Stereotypic wheel running decreases cortical activity in mice. *Nat Comm* **7**, 13138 (2016). https://doi.org/10.1038/ncomms13138

48 Shimaoka, D., Harris, D. K. & Carandini, M. Effects of Arousal on Mouse Sensory Cortex Depend on Modality. *Cell Rep* **22**, 3160-3167 (2018). https://doi.org/10.1016/j.celrep.2018.02.092

49 Christensen, J. A. & Pillow, W. J. Reduced neural activity but improved coding in rodent higher-order visual cortex during locomotion. *Nat Comm* **13**

(2022). https://doi.org/10.1038/s41467-022-29200-z

50 Schneider, M. D., Nelson, A. & Mooney, R. A synaptic and circuit basis for corollary discharge in the auditory cortex. *Nature* **513**, 189-194 (2014). https://doi.org/10.1038/nature13724

51 McCormick, D. A. Cholinergic and noradrenergic modulation of thalamocortical processing. *Trends in neurosciences* **12**, 215-221 (1989). https://doi.org/10.1016/0166-2236(89)90125-2

52 Eggermann, E., Kremer, Y., Crochet, S. & Petersen, C. C. H. Cholinergic signals in mouse barrel cortex during active whisker sensing. *Cell Rep* **9**, 1654-1660 (2014). https://doi.org/10.1016/j.celrep.2014.11.005

53 Chen, N., Sugihara, H. & Sur, M. An acetylcholine-activated microcircuit drives temporal dynamics of cortical activity. *Nat Neurosci* **18**, 892-902 (2015). https://doi.org/10.1038/nn.4002

54 Rauscher, C. B. *et al.* (2024).

55 Inácio, R. A. *et al*. Brain-wide presynaptic networks of functionally distinct cortical neurons. *Nature* (2025). https://doi.org/10.1038/s41586-025-08631-w

56 Cauli, B. *et al*. Cortical GABA Interneurons in Neurovascular Coupling: Relays for Subcortical Vasoactive Pathways. *J Neurosci* **24**, 8940-8949 (2004). https://doi.org/10.1523/JNEUROSCI.3065-04.2004

57 Gentet, J. L., Avermann, M., Matyas, F., Staiger, F. J. & Petersen, C. H. C. Membrane Potential Dynamics of GABAergic Neurons in the Barrel Cortex of Behaving Mice. *Neuron* **65**, 422-435 (2010). https://doi.org/10.1016/j.neuron.2010.01.006

58 Gentet, L. J. *et al*. Unique functional properties of somatostatin-expressing GABAergic neurons in mouse barrel cortex. *Nat Neurosci* **15**, 607-612 (2012). https://doi.org/10.1038/nn.3051

59 Fu, Y. *et al*. A cortical circuit for gain control by behavioral state. *Cell* **156**, 1139-1152 (2014). https://doi.org/10.1016/j.cell.2014.01.050

60 Muñoz, W., Tremblay, R., Levenstein, D. & Rudy, B. Layer-specific modulation of neocortical dendritic inhibition during active wakefulness. *Science* **355**, 954-959 (2017). https://doi.org/10.1126/science.aag2599

61 Mayerich, D., Abbott, L. & McCormick, B. Knife-edge scanning microscopy for imaging and reconstruction of three-dimensional anatomical structures of the mouse brain. *Journal of Microscopy* **231**, 134-143 (2008). https://doi.org/https://doi.org/10.1111/j.1365-2818.2008.02024.x

62 Ragan, T. *et al*. Serial two-photon tomography for automated ex vivo mouse brain imaging. *Nat Methods* **9**, 255-258 (2012). https://doi.org/10.1038/nmeth.1854

63 Demené, C. *et al*. Spatiotemporal Clutter Filtering of Ultrafast Ultrasound Data Highly Increases Doppler and fUltrasound Sensitivity. *IEEE Transactions on Medical Imaging* **34**, 2271-2285 (2015). https://doi.org/10.1109/TMI.2015.2428634

64 Pnevmatikakis, A. E. & Giovannucci, A. NoRMCorre: An online algorithm for piecewise rigid motion correction of calcium imaging data. *J Neurosci Methods* **291**, 83-94 (2017). https://doi.org/10.1016/j.jneumeth.2017.07.031

65 Tyson, L. A. *et al*. Accurate determination of marker location within whole-brain microscopy images. *Sci Rep* **12** (2022). https://doi.org/10.1038/s41598-021-04676-9

66 Niedworok, J. C. *et al*. aMAP is a validated pipeline for registration and segmentation of high-resolution mouse brain data. *Nat Comm* **7**, 11879 (2016). https://doi.org/10.1038/ncomms11879

67 Claudi, F. *et al*. BrainGlobe Atlas API: a common interface for neuroanatomical atlases. *Journal of Open Source Software* **5**, 2668 (2020). https://doi.org/10.21105/joss.02668